

RESEARCH ARTICLE

Spatiotemporal climate variability in the Andes of northern Peru: Evaluation of gridded datasets to describe cloud forest microclimate and local rainfall

Felicity L. Newell^{1,2}  | Ian J. Ausprey^{1,2}  | Scott K. Robinson¹

¹Florida Museum of Natural History & Department of Biology, University of Florida, Gainesville, Florida, USA

²Current address: Division of Conservation Biology, Institute of Ecology and Evolution, University of Bern, Bern, Switzerland

Correspondence

Felicity Newell, Division of Conservation Biology, Institute of Ecology and Evolution, Erlachstrasse 9a, 3102 Bern, Switzerland.

Email: fnewell@ufl.edu; felicity.newell@gmail.com

Funding information

Florida Museum of Natural History, Grant/Award Number: Katharine Ordway Chair of Ecosystem Conservation; Idea Wild, Grant/Award Number: Equipment Funding; University of Florida, Grant/Award Numbers: CLAS Dissertation Fellowship, Grinter Fellowship

Abstract

Tropical montane cloud forest may be especially sensitive to climate change. However, our ability to understand effects of climate on montane biodiversity remains limited by the resolution of climate data. We compared 5 years of in situ weather data from cloud forests in northern Peru, regional weather stations, and gridded datasets to examine how climatologies reflect (a) forest microclimate buffering and (b) local rainfall in a sparse data region; we also examined spatiotemporal variability and regional trends. Across a 1,700–3,100 m gradient in which temperature did not covary with relative humidity (RH), in situ data showed interactions between climate and land-use. Forest humidity buffered warming-induced evaporative drying across elevations, and inside forest maximum vapour pressure deficit (VPD_{max}) did not change with elevation, whereas with a 22% reduction in RH_{min} at stations, VPD_{max} increased >10-fold from high to low elevations. Cloud forest dried out on sunny days after 3 days without rain, especially during ENSO-related drought concurrent with peak solar insolation. Climatologies were twice as precise for temperature as rainfall. Chelsa captured a 3.9°C reduction in maximum temperatures inside forest (MAE 1.6°C, $R^2 = 0.95$) whereas WorldClim reflected drier lapse rates and higher T_{max} outside forest. CHIRPS provided the best fit for monthly rainfall (MAE 23 mm, $R^2 = 48$), capturing regional drought but underestimating rainfall >150 mm·month⁻¹. Consistent with stations, CHIRPS showed strong support for regional increases in wet-season rainfall. Reduced variability and more regular dry seasons were only detected by montane stations, especially south of 6°S, where rainfall seasonality shifted to earlier wet-season peaks and reduced dry-season rainfall as part of a transition from the Northern to Central Andes. Our results show that cloud forests may be partly buffered from warming but are likely to become extremely vulnerable under reduced humidity either through forest loss or drought.

KEYWORDS

Andes, climatologies, drought, elevational gradient, forest microclimate, rainfall seasonality, temperature lapse rate, tropical montane cloud forest

This is an open access article under the terms of the [Creative Commons Attribution](https://creativecommons.org/licenses/by/4.0/) License, which permits use, distribution and reproduction in any medium, provided the original work is properly cited.

© 2022 The Authors. *International Journal of Climatology* published by John Wiley & Sons Ltd on behalf of Royal Meteorological Society.

1 | INTRODUCTION

In an era of big data, the last decade has seen a rapid increase in the number of global climatologies combining station and satellite-based data to interpolate and down-scale temperature and rainfall as easily accessible gridded high-resolution datasets (Funk *et al.*, 2015; Fick and Hijmans, 2017; Karger *et al.*, 2017; Abatzoglou *et al.*, 2018a). Since the original WorldClim (Hijmans *et al.*, 2005), recent improvements provide more comprehensive global datasets on moisture regimes at 1-km scales including vapour pressure (Fick and Hijmans, 2017), improved precipitation downscaling for mountainous terrain from Chelsa (Karger *et al.*, 2017), as well as refined regional grids such as PISCO for Peru (Aybar *et al.*, 2020). Additional daily precipitation time series are available at 0.05° resolution from CHIRPS (Funk *et al.*, 2015) with 30-min precipitation at 0.1° resolution from GPM-IMERG (Huffman *et al.*, 2019). However, despite their usefulness, global gridded datasets often reflect forest microclimate poorly (Faye *et al.*, 2014; Lembrechts *et al.*, 2019; Montejo-Kovacevich *et al.*, 2020). Additionally, uncertainties in areas with a low density of weather stations remain a challenge, especially sparse data in mountainous regions where heterogeneous topography contributes to local variation in climate (Bobrowski *et al.*, 2021).

The problem of lack of on-the-ground data is accentuated in biodiversity studies, as station-based weather data often come from populated often drier areas (Fick and Hijmans, 2017), whereas high biodiversity is typically found in remote forested mountains. For example, 85% of terrestrial vertebrate species are estimated to be compacted into only 25% of the global land area in mountains (Rahbek *et al.*, 2019). Among the most hyperdiverse systems in the world, the tropical Andes are estimated to occupy half of the world's climate space (Rahbek *et al.*, 2019) and this region is considered an important “biodiversity hotspot” for conservation because of many range-restricted flora and fauna (Myers *et al.*, 2000). However, in the Central Andes of Peru and Bolivia known as the Yungas, global climatologies may be based on as few as two to seven stations compared to often >20 stations per 10,000 km² in the northern Andes of Ecuador, Colombia, and Venezuela (Fick and Hijmans, 2017).

In the context of climate change, mountains become even more important as refugia from warming. The prevailing paradigm is that species are shifting upslope although the rate of change often lags behind warming (Colwell *et al.*, 2008; Feeley *et al.*, 2011; Forero-Medina *et al.*, 2011; Freeman and Class Freeman, 2014; Lenoir and Svenning, 2015; Fadrique *et al.*, 2018; Freeman *et al.*, 2018; 2021; Feeley *et al.*, 2020) which may be explained by forest microclimate buffering (Zellweger

et al., 2020). Studies often use global climatologies to model distributional shifts in response to climate change (Feeley *et al.*, 2020; Freeman *et al.*, 2021). However, humid systems such as tropical montane cloud forest may be especially threatened by subtle changes in moisture regimes, such as reductions in cloud immersion (Still *et al.*, 1999; Foster, 2001; Bruijnzeel *et al.*, 2011; Helmer *et al.*, 2019). Cloud forest epiphytes are highly dependent on moist air (Nadkarni and Solano, 2002; Gotsch *et al.*, 2017), and ocean warming related drying of cloud forests have been documented in Costa Rica (Pounds *et al.*, 1999; Karmalkar *et al.*, 2008) and México (Ponce-Reyes *et al.*, 2012).

Terrestrial drying depends on precipitation and evapotranspiration (Cook *et al.*, 2014; Sherwood and Fu, 2014; Padrón *et al.*, 2020). Idealized thermodynamics predict intensification of the hydrologic cycle, the “wet get wetter and dry get drier” hypothesis (Held and Soden, 2006), but challenges remain to understanding continental moisture transport (Gimeno *et al.*, 2020). Reduced dry season water availability has been attributed to human-induced warming (Padrón *et al.*, 2020), but uncertainties in the demand side of drought models fuel debate about whether droughts are increasing (Ault, 2020; Vicente-Serrano *et al.*, 2020). In the absence of changes to solar insolation or windspeed, potential evapotranspiration and atmospheric evaporative demand relate to vapour pressure deficit (VPD), or the “drying power of the air,” measured as the difference between actual water vapour and vapour pressure saturation (VP_{sat}) (Penman, 1948; Monteith, 1965). Critically, VP_{sat} increases with temperature approximately 7% per 1°C according to the Clausius–Clapeyron relation (Held and Soden, 2006). Unlike relative humidity (RH), VPD provides a linear measure of the exponential relationship between temperature and evapotranspiration (Anderson, 1936), and increasing VPD around the globe has been linked to reduced vegetation growth (Yuan *et al.*, 2019) and wildfires (Abatzoglou *et al.*, 2018b).

Local climatic conditions experienced by biodiversity are influenced by temperature–moisture feedbacks across multiple scales. Warming increases evaporation, but as liquid water vaporizes, energy becomes stored as latent heat contributing to cloud cover which further regulates surface temperatures. Globally, night-time warming is increasing faster than daytime warming associated with increased cloud cover, humidity, and precipitation (Davy *et al.*, 2017; Cox *et al.*, 2020). Forest transpiration results in evaporative cooling (Bonan, 2008) and forest microclimates buffer near-surface temperature extremes (De Frenne *et al.*, 2019), especially in the understory (Davis *et al.*, 2019). Forests also contribute vegetation–atmosphere feedbacks (Zemp and Rammig, 2014; Zemp *et al.*, 2017) as moisture recycling from transpiration

reduces downwind rainfall variability around the globe (O'Connor *et al.*, 2021).

Although moisture regimes play a critical role in ecosystem function, relatively few studies have examined climatic variability across elevational gradients in humid low-latitude mountains (Duane *et al.*, 2008; Fries *et al.*, 2009; Rapp and Silman, 2012; Ramírez *et al.*, 2017; Jucker *et al.*, 2018). Here we compare 5 years of data on cloud forest microclimate and local rainfall with regional weather stations outside forest to examine drivers of variation in montane climate. We then examine how cloud forest climate is reflected by several global climatologies commonly used for species distributional modelling. Our objectives were to (1) examine microclimate buffering of forest including (1a) compare temperature extremes and lapse rates inside versus outside forest to gridded climatologies (WorldClim, Chelsa); (1b) identify drivers of cloud forest evaporative drying testing the prediction that VPD increases at warmer lower elevation because of higher VP_{sat} ; (2) evaluate reliability of gridded precipitation datasets to measure spatiotemporal rainfall variability in a sparse data region (WorldClim, Chelsa, CHIRPS, GPM-IMERG, PISCO); and (3) examine effects of climate change on cloud forests in northern Peru (drought, inter-annual variability, trends). Analyses integrate data from local, regional, and global scales to provide insight on cloud forest and montane climate relevant for biodiversity conservation (Figure 1).

2 | DATA AND METHODS

2.1 | Cloud forest and regional weather stations in northern Peru at 5°–7°S

Our study was conducted at a transition between the Northern and Central Andes (Figure 2a), where the

Cordillera Oriental and Central break up around the Marañón River valley and Huancabamba Depression, a well-known biogeographic divide where elevation drops to 500–2,100 m (Weigend, 2002; Hazzi *et al.*, 2018). The region is characterized by extreme topographic complexity with seasonal temperature differences $<2^{\circ}\text{C}$. Orographic lift combined with rain-shadow effects and narrow canyons result in rainforest, dry forest, and cloud forest in proximity. Weather data used in our analysis reflect this climatic variability at small spatial scales, and we compared cloud forests ($n = 8$) in a $2^{\circ} \times 2^{\circ}$ gridded area between 5° – 7°S and 77 – 79°W to regional weather stations within 100 km ($n = 32$ – 46) (Figure 2a). Stations covered a range of slope and aspect with cloud forest generally accessible on moderate mid-slopes near rural communities (Figure S1, Supporting Information).

To examine forest microclimate and local rainfall, we used 5 years of data collected in cloud forest as part of a larger study examining the interaction of climate and land-use on biodiversity (Ausprey *et al.*, 2020; Newell, 2021). Cloud forest spanned a 1,700–3,100 m elevational gradient (Tmean 10 – 17°C) across a 10,000 km² area in the vicinity of the city of Chachapoyas (Figure 2a and Tables S1–S4), and mean annual precipitation ranged from 1,000–2,500 mm (Figure 2d, Tables S2–S4). At inter-Andean sites dry seasons based on water stress ranged from 2.7 to 4.7 months (82–142 days) compared to less than 1 month of water stress on the eastern slopes. Weather data were collected at eight landscapes across four watersheds including the Utcubamba and Imaza, tributaries of the Marañón; and Huayabamba and Mayo, tributaries of the Huallaga. Based on vegetation plots at >40 stands, forest microclimate represented typical cloud forest in the region characterized by 71–91% canopy closure (spherical densiometer) with 12–21 m tall canopies in which height decreased slightly with elevation.

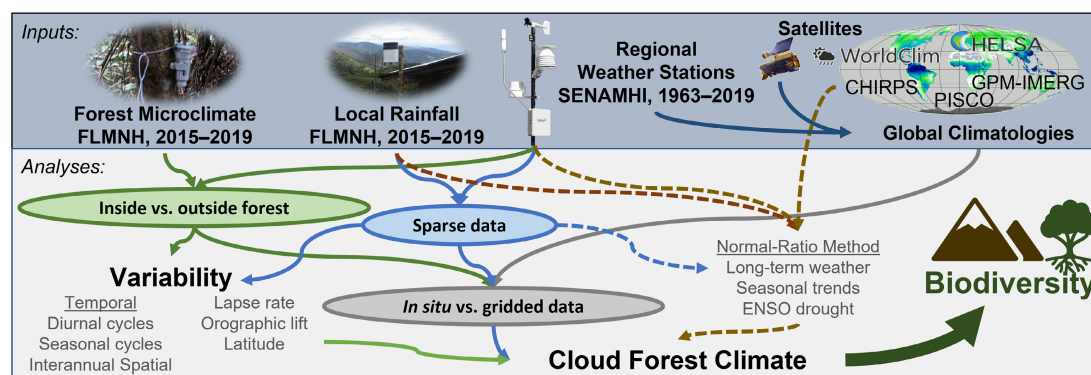


FIGURE 1 Flow chart of data inputs and analytical comparisons examining spatiotemporal variability and reliability of gridded global climatologies to describe tropical montane cloud forest climate in the context of biodiversity studies. Weather data from the Florida Museum of Natural History (FLMNH) and stations maintained and compiled by the Peruvian National Meteorology and Hydrology Service (SENAMHI) [Colour figure can be viewed at [wileyonlinelibrary.com](https://onlinelibrary.wiley.com/doi/10.1002/joc.7567)]

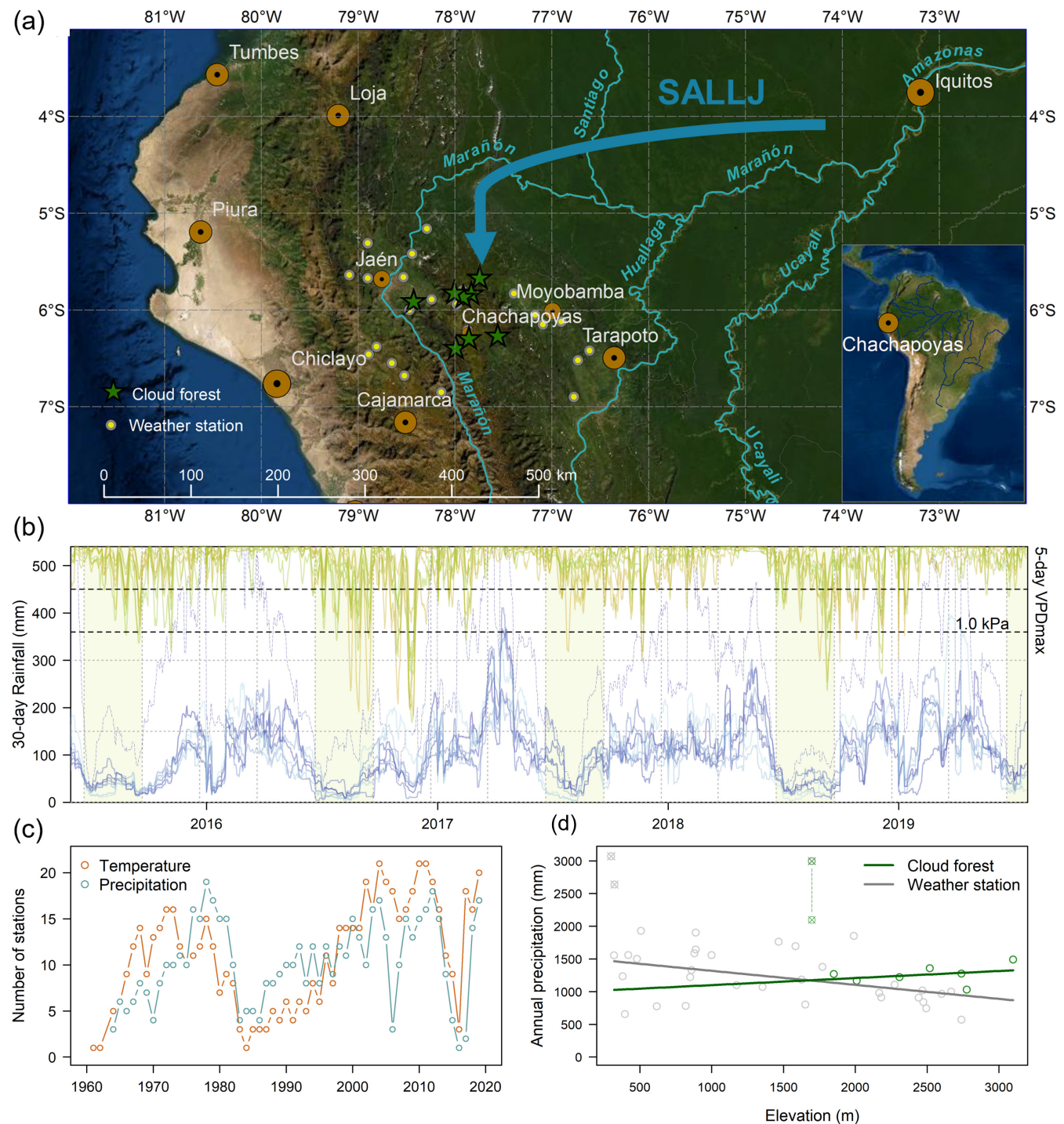


FIGURE 2 Spatiotemporal weather data in northern Peru at a climatic transition between the Northern and Central Andes, and the eastern slopes and inter-Andean ridges. (a) Map of a network of cloud forest sites (stars) and long-term regional weather stations (circles) within 100 km; prevailing winds from the South American low-level jet (SALLJ) shown in blue. (b) Variation in rainfall and maximum vapour pressure deficit (VPDmax) at cloud forest sites across a complex 1,700–3,100 m elevation gradient from 2015–2019; shaded areas represent the austral winter (dry season). (c) Number of regional weather stations by year from SENAMHI. (d) Mean annual precipitation by elevation for cloud forest and weather stations; hatched circles represent sites on the eastern slopes with dashed lines for approximate rainfall [Colour figure can be viewed at [wileyonlinelibrary.com](https://onlinelibrary.wiley.com)]

In situ weather data were collected in cloud forests from 2015–2019, including a strong El Niño event in 2015–16, as well as weak El Niño conditions in 2018–19

(Figure 2b). To measure microclimate inside forest, weather loggers were attached to a tree 1.5 m above the ground in a dense closed-canopy area (loggers were

concealed at accessible stands away from trails and edges). At each landscape a pair of Onset HOBO loggers recorded temperature/RH every 30 min (U23-001) and temperature/lux (UA-002) every 15 min; light loggers were attached above humidity loggers with sensors oriented horizontally to capture ambient light while avoiding spikes from direct sunlight. In a nearby open area, Onset HOBO tipping-bucket rain gauges (RG3-M) recorded local precipitation at each landscape, here defined as rainfall; we did not measure cloud water interception, which can be highly variable (Giambelluca and Gerold, 2011). Coverage per year ranged from 78 to 95% due to occasional logger failures, and data collection at one landscape was discontinued in 2016 due to safety concerns while two additional landscapes were added the same year (Table S1).

Regional weather stations were located within 100 km of cloud forest sites and spanned a 300–3,100 m elevational gradient in the departments of Amazonas, San Martín, and Cajamarca (Figure 2a). Stations included rainforest and dry forest as well as cloud forest with mean annual precipitation ranging from 500–3,000 mm (Table S5). We downloaded meteorology data compiled and maintained by the Peruvian National Meteorology and Hydrology Service (*Servicio Nacional de Meteorología e Hidrología* SENAMHI, <http://www.senamhi.gob.pe>) using the R package *senamhiR* (Anderson, 2018). Data were graphed and scanned for consistency, and we dropped one station with unreliable RH. For analysis we used 32–46 stations with >9 years of data (Table S5); about half were located >1,500 m ($n = 23$). Records at the longest running stations began in the early 1960s (Figure 2c) primarily from populated, often drier areas. Seven weather stations were located within the 10,000 km² cloud forest network, but three have been inactive for >30 years (Table S5). Classified as a humid highland climate (*Cfb*) according to the Köppen climate classification, at 2,400 m the city of Chachapoyas is the only montane station with >50 years of data, although coverage has been incomplete. Universidad Nacional Toribio Rodríguez de Mendoza de Amazonas is developing an improved network of weather stations (Rojas Briceño *et al.*, 2021).

2.2 | Global gridded climatologies

We selected two commonly used global climatologies to compare with in situ data. WorldClim uses a thin-plate smoothing spline to interpolate climate surfaces at a 1-km scale based on geographic location and elevation (Hijmans *et al.*, 2005), and v2.1 has been refined to include additional stations, other factors such as cloud

cover and distance to ocean, as well as high-resolution datasets for vapour pressure to model complex processes involved in evapotranspiration (Fick and Hijmans, 2017). Using an improved downscaling approach to estimate precipitation in mountainous regions, Chelsa v2.1 provides a similar 1-km scale resolution for temperature and precipitation (Karger *et al.*, 2017; 2021).

We also examined several gridded precipitation time series. CHIRPS v2.0 (<https://data.chc.ucsb.edu/products/CHIRPS-2.0/>) provides daily precipitation since 1981 at a 0.05° × 0.05° scale resolution that can be used for trend analysis (Funk *et al.*, 2015). GPM-IMERG v6.0 from NASA provides 30-min precipitation since 2000 at a 0.1° × 0.1° scale (Huffman *et al.*, 2019). This dataset joins satellite data from the current Global Precipitation Measurement (GPM) since 2014 with the Tropical Rainfall Measuring Mission from 2000 to 2015 (TRMM). For analyses we used Final Run monthly precipitation accumulation datasets available in GeoTIFF format (<https://arthurhou.pps.eosdis.nasa.gov/>). We also examined refined regional precipitation grids for Peru from PISCO v2.1 (Aybar *et al.*, 2020). For trend analysis we only examined time series from CHIRPS as other time series are not considered appropriate because of data inhomogeneities.

For comparison, we extracted point-level data for coordinates using bi-linear interpolation in R with the raster (Hijmans, 2020), *ncdf4* (Pierce, 2019), and *chirps* (de Sousa *et al.*, 2020) packages or using the ArcGIS Spatial Analyst multivalue to points tool. For precipitation datasets, we calculated annual and monthly normals for comparison with WorldClim (<https://www.worldclim.org/data/worldclim21.html>) and Chelsa (<https://chelsa-climate.org/downloads/>). Cloud cover was downloaded from MOD09GA (<https://lpdaac.usgs.gov/products/mod09gav061/>) at a 250 m resolution (Vermote and Wolfe, 2015) and we calculated the percentage of total pixels occupied by cloud within a 5-km radius buffer of rain gauges.

2.3 | Data formatting and statistical analysis

Cloud forest and weather station data were formatted on a daily time step for comparison. Forest logger data were averaged per hour, and we extracted daily minima, maxima, and means. We calculated means as the sum of extremes divided by two to be comparable with stations which reported data for 700, 1300, and 1900 hrs. Forest loggers did not record RH > 100%, but supersaturation with dew can affect around 6% of high humidity measurements (Rapp and Silman, 2012). For stations, we calculated RH from dry and wet bulb temperatures plus

atmospheric pressure based on elevation and temperature, and we calculated VPD from temperature, RH, and pressure using the R package *psychrolib* (Meyer and Thevenard, 2019). To examine logger cloud cover, we calculated relative light levels as the proportion of trimmed maxima by sensor controlling for variation in light based on placement. For trimmed maxima we used 95th percentiles to replace extreme values when direct sunlight occasionally filtered through leaves (winsorizing). For each metric we calculated daily running means and sums by 5-day, 10-day, 30-day, and 90-day increments using the R package *data.table* (Dowle and Srinivasan, 2020).

We used daily data to examine temperature lapse rates and dry season length. We calculated near-surface lapse rates inside versus outside forest by day for T_{min}, T_{mean}, and T_{max} then averaged by month and year (Rapp and Silman, 2012); only days with data from ≥ 5 loggers were included in the analysis (Lute and Abatzoglou, 2021). We used two approaches to calculate dry season length at cloud forest sites, either below average rainfall or based on water stress. Similar to approaches used in tropical rainforest (Fu *et al.*, 2013), we considered start/end of the dry season based on 6/8 pentads below normal 5-day mean rainfall for the site. Additionally, we considered start/end of the dry season based on five consecutive days of water stress. We calculated daily water stress as negative climatic water balance ($-CWB$) using the Thornthwaite equation for temperature to calculate potential evapotranspiration (PET): $CWB = Precip_{30days} - PET_{30days}$ (Thornthwaite, 1948; Vicente-Serrano *et al.*, 2010).

We compared gridded climatologies to observed data based on monthly normals averaged across years by site. Because of sparse in situ data, we did not limit our comparison to concurrent years. For cloud forest we used monthly means from the normal ratio method (see below) for the 1970–2019 time period, and for stations we used all years with data. Any weak effects of trends (see below) were likely outweighed by more robust sample sizes. Results were similar although weaker for 12 stations $>1,500$ m which were active concurrent with our cloud forest network from 2015 to 2019. We evaluated gridded climatologies based on mean directional differences (intercepts centred by group), slope of the line (1:1 ratios), proportion of variation explained (R^2), and mean absolute error (MAE) calculated using the Metrics package in R (Hamner *et al.*, 2018). We present 95% confidence intervals (CI) from the emmeans package (Lenth, 2020).

Statistical analyses were conducted in Program R. Prior to analysis we examined Pearson correlation coefficients among weather variables. We used maximum likelihood linear, generalized linear, or generalized additive mixed models with the lme4 (Bates *et al.*, 2015) or gamm4

packages (Wood and Scheipl, 2020). To examine forest buffering of climatic extremes, we compared daily ranges inside versus outside forest using kernel density estimates. We used AIC_c model selection to compare relative importance of factors contributing to hot and dry extremes (T_{max}, RH_{min}, VPD_{max}) with repeated measures by landscape and year. For VPD_{max} we used a Gamma distribution with a log link function which provided the best fit for right-skewed data; a few zero months were replaced with a minimal value (0.0001). Across the region we examined logger location (inside vs. outside forest) as an interactive effect. Partial regressions from top models were visualized using the visreg package (Breheny and Burchett, 2017) and we used the rr2 package (Ives and Li, 2018) to examine the proportion of variation explained.

2.4 | Normal ratio method, interannual variability, and regional trends

In montane regions, the normal ratio method provides a better predictor of local rainfall than inverse distance weighting (Paulhus and Kohler, 1952; Mair and Fares, 2010) typically used for interpolating gridded datasets (Fick and Hijmans, 2017; Aybar *et al.*, 2020). With sparse data, we integrated local and regional weather data to model interannual variability over 50 years scaled to cloud forest sites; models generally provided a good fit to the data (Table S11 and Figures S6 and S7). On the eastern slopes of the Andes at the Venceremos guard station in Bosque de Protección Alto Mayo (BPAM), we recorded 2,775 mm of rain in 324 days during El Niño when other sites were drier than normal. Extensive landslides suggest there was an inverse ENSO effect, and for analyses we scaled Venceremos rainfall models by 70% to allow for comparison across sites (Figure 2d, S2 and Table S3-4). For a few months in which loggers malfunctioned or prior to installation at all sites, we estimated daily temperature and RH using the normal ratio method; daily values were used to calculate VPD. See Data S1, Supporting Information for details.

We examined seasonal trends in temperature and rainfall for regional weather stations with >9 years of data. We examined decadal changes from regression models (mean) and Sen's slope (median) with the R package *trend* which allows for nonlinearities and reduces effects of outliers (Thorsten, 2020). For temperature, we used linear regression to examine trends in daily means and extremes. For rainfall, we examined trends in 30-day rainfall accumulation using a Gamma distribution with a log link function as variance typically increases with the mean (Husak *et al.*, 2007).

3 | RESULTS

3.1 | Microclimatic buffering effects of forests

3.1.1 | Temperatures inside versus outside forest compared to gridded climatologies

Forest microclimate reduced climatic variability. Cloud forests were characterized by high nocturnal humidity year-round, although daytime RH and VPD varied by season (Figure 3). Increasing solar insolation after the winter solstice contributed to greater temperature extremes combined with potential water stress from July to December (Figure 4). Inside forest, daily thermal ranges were reduced by half compared to regional weather stations while forest microclimate buffered evaporative drying under most conditions (Figure 5). Temperatures inside forest were systematically offset compared to stations. Controlling for elevation, forest Tmin was 0.7°C (CI 0.1–1.3) warmer than stations, whereas forest Tmean and Tmax were 2.0°C (CI 2.5–1.4) and 3.9°C (CI 3.0–4.8) cooler, respectively.

Cloud forest microclimate reduced near-surface lapse rates up to 0.8°C·km⁻¹ (Figure 6a). Greatest differences

were for Tmax, and Tmax lapse rates inside forest were 4.8°C·km⁻¹ (CI 4.9–4.7) compared to 5.6°C·km⁻¹ (CI 5.7–5.5) outside forest. Effects of forest microclimate decreased for Tmean at 4.5°C·km⁻¹ (CI 4.6–4.4) compared to 5.3°C·km⁻¹ (CI 5.3–5.2), and Tmin at 4.2°C·km⁻¹ (CI 4.3–4.1) compared to 4.9°C·km⁻¹ (CI 5.0–4.8). For most of the year forest Tmin and Tmax lapse rates were similar, but in September at the end of the dry season, forest Tmax lapse rates were reduced >1°C matching drier lapse rates of stations, whereas Tmin lapse rates remained relatively constant throughout the year (Table S5 and Figure S3).

Cooling effects of forest microclimate were reflected by Chelsa whereas WorldClim was most accurate outside forest (Figure 6b,c). Based on centred intercepts (Table S9), monthly normals for Tmin were well predicted by grids independent of dataset or location within -1.1 to 0.4°C (MAE 0.8–1.2). WorldClim predicted Tmean and Tmax outside forest within -0.3 to 0.3°C (MAE 0.8–1.2) but increasingly overestimated Tmean and Tmax inside forest by 2.1°C (MAE 2.1) and 4.0°C (MAE 4.0), respectively. Chelsa balanced Tmean between locations at -0.7 to 1.1°C (MAE 0.7–1.1) and corrected overestimation of forest Tmax within 0.2°C (MAE 1.6), but underestimated Tmax outside forest by 2.3°C (MAE 2.4). In v2.1 Tmax increased linearly with observed values (1:1 ratio 0.95), an

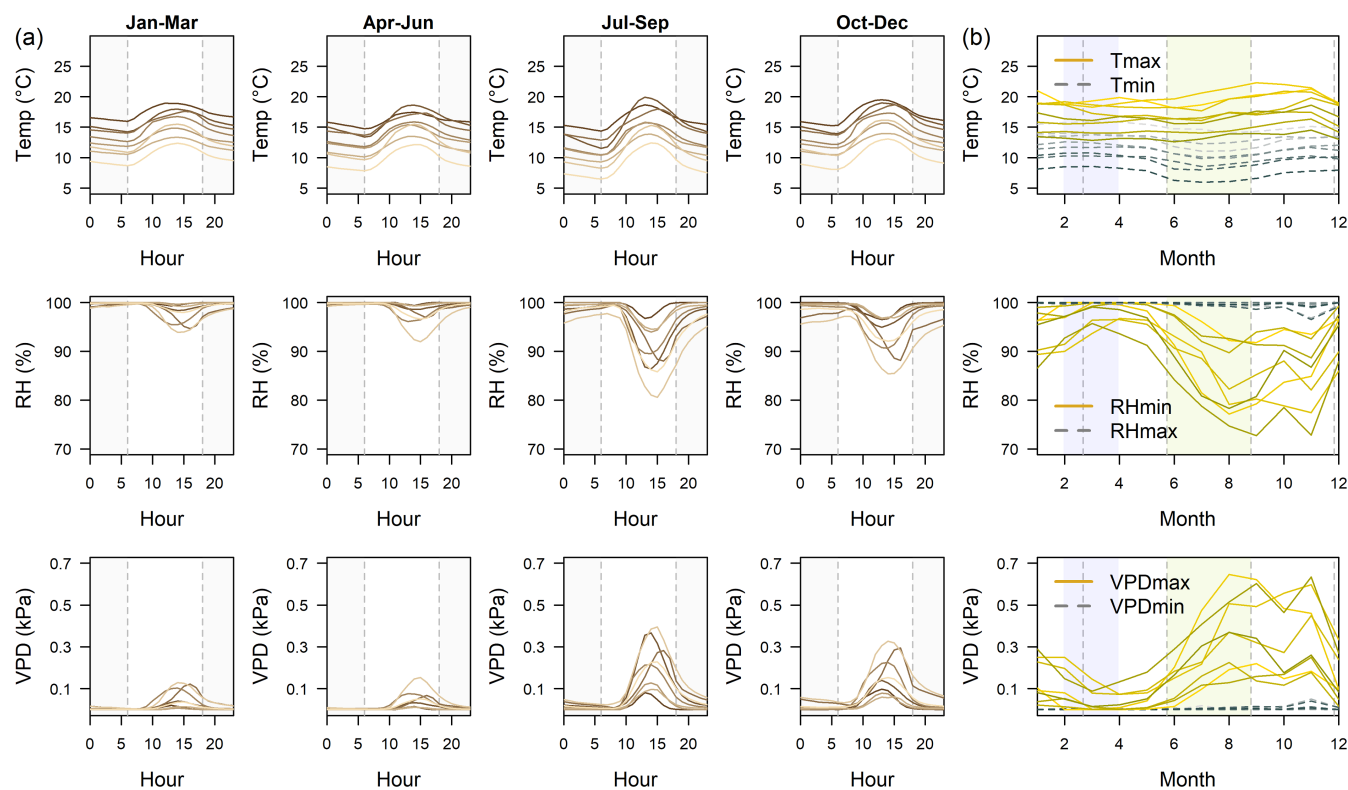


FIGURE 3 Diurnal and seasonal cycles in temperature, relative humidity (RH), and vapour pressure deficit (VPD) inside cloud forest for a network of sites ($n = 8$, 2015–2019) across a 1,700–3,100 m elevational gradient in the Chachapoyas region of northern Peru. Hourly means by quarter (a) and mean monthly extremes (b). Shaded areas represent night-time, or wet (blue) and dry (tan) seasons [Colour figure can be viewed at [wileyonlinelibrary.com](https://onlinelibrary.wiley.com)]

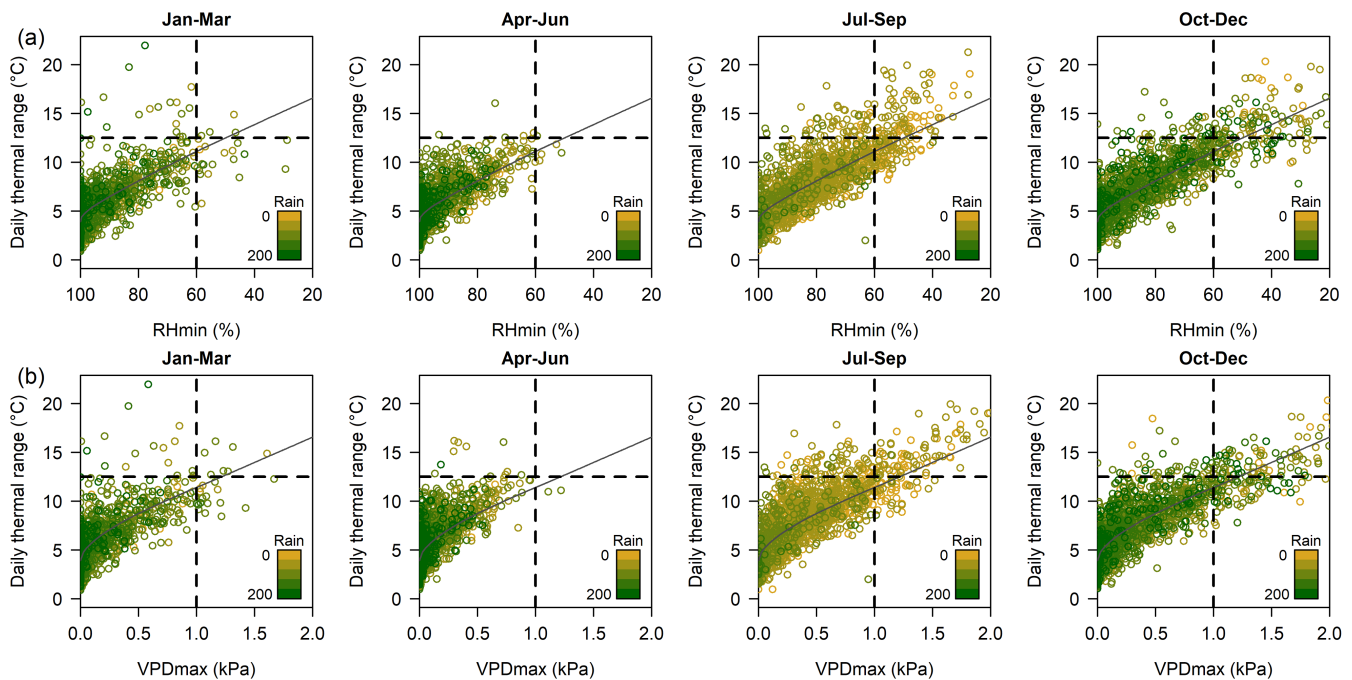


FIGURE 4 Seasonal daily thermal range inside cloud forest by (a) minimum relative humidity (RHmin), and (b) maximum vapour pressure deficit (VPDmax) in relation to 30-day rainfall accumulation for a network of sites ($n = 8$, 2015–2019) in the Chachapoyas region of northern Peru. Black dashed lines represent 95th-percentile ranges for the least variable quarter April–June after the rainy season [Colour figure can be viewed at [wileyonlinelibrary.com](https://onlinelibrary.wiley.com/doi/10.1002/joc.7567)]

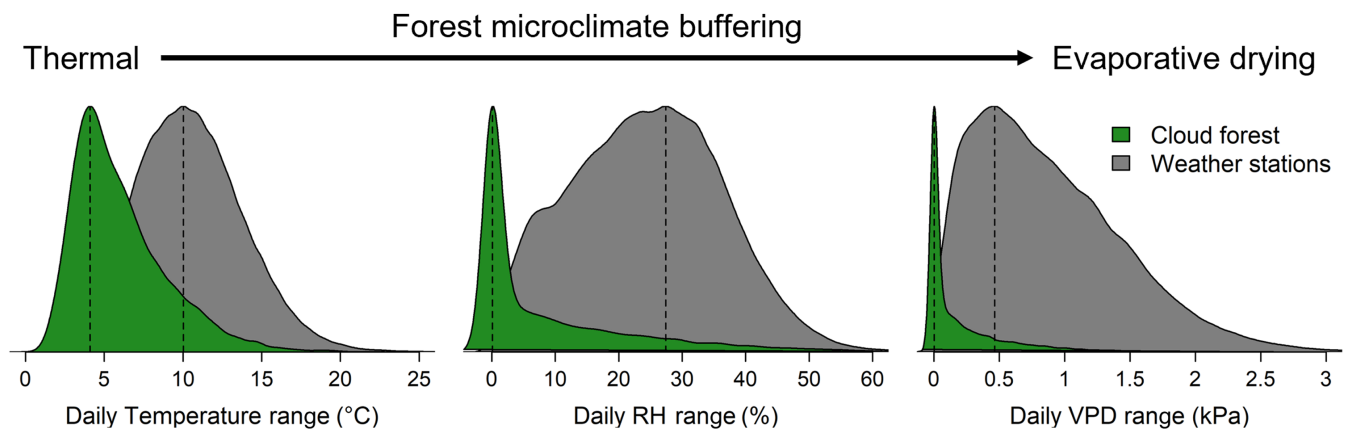


FIGURE 5 Buffering effects of forest microclimate on the range of daily climatic variability inside versus outside forest for temperature, relative humidity (RH) and vapour pressure deficit (VPD). Polygons represent overlay of kernel density estimates scaled to maximum values for a network of cloud forest sites ($n = 8$, 2015–2019) and regional weather stations ($n = 32$, 1963–2019) in northern Peru [Colour figure can be viewed at [wileyonlinelibrary.com](https://onlinelibrary.wiley.com/doi/10.1002/joc.7567)]

improvement over WorldClim and previous versions (Table S9). Temperature models provided a good fit to the data explaining 94–98% of the variation (Table S9).

3.1.2 | Forest humidity buffers warming-induced drying across elevations

Reduced rainfall combined with high solar insolation contributed to cloud forest evaporative drying in conjunction with regular diurnal and seasonal cycles (Figures 3 and 4).

During the second half of the year, forest VPDmax increased on dry, sunny days, especially after at least 3 days without rain, but not without the combination of both factors (Figure 7a). When controlling for season, rainfall was the top predictor for mean monthly VPDmax across elevations (Figure 7b and Table S8); inside forest, season explained 20% of the variation with an additional 18% explained by rainfall and 6% explained by El Niño. However, effects of rainfall alone were weak and for both cloud forest and weather stations, RHmin increased 13% across a rainfall range of 0–300 mm-month⁻¹ whereas

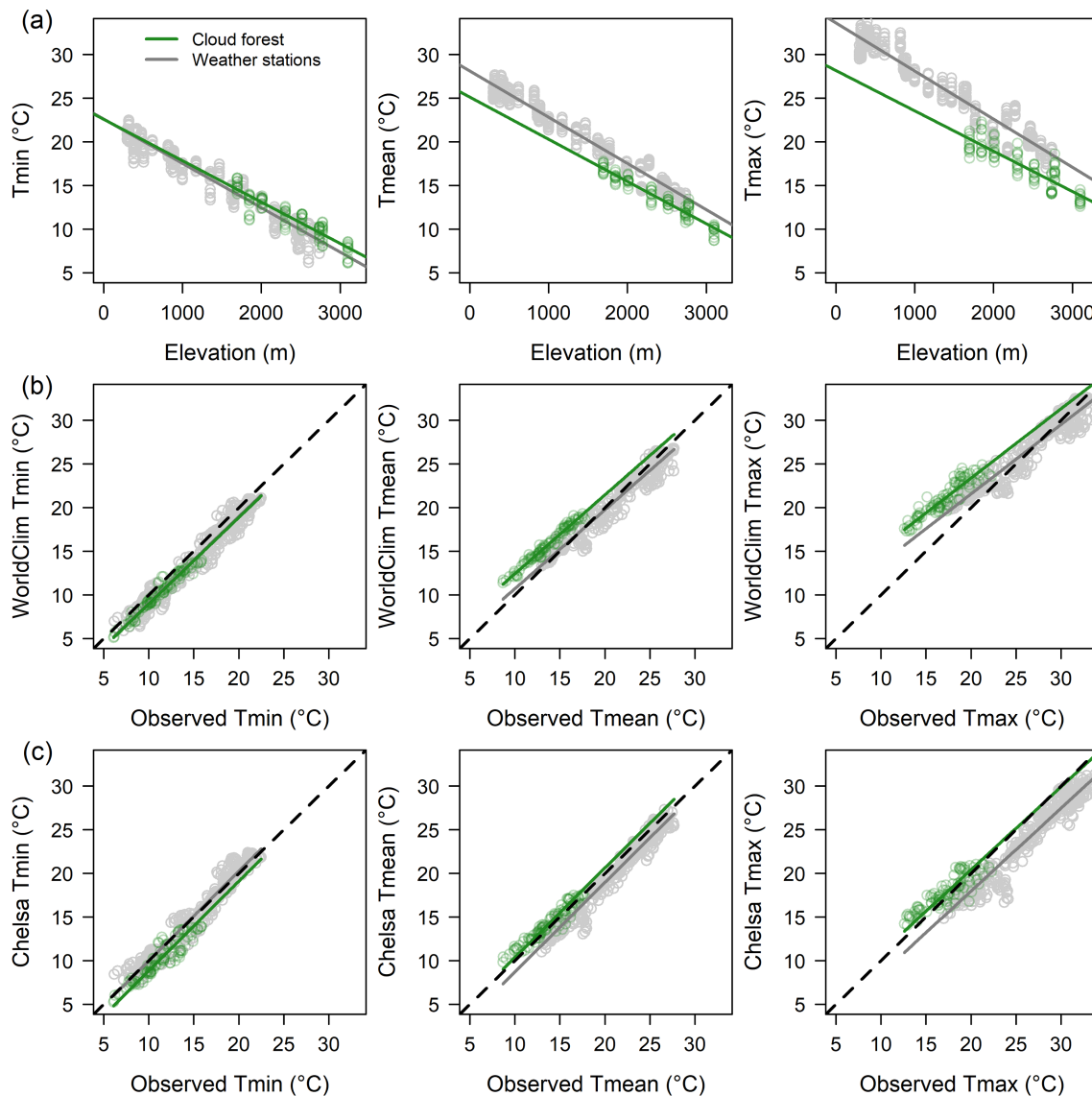


FIGURE 6 Observed minimum, mean, and maximum monthly temperatures inside vs. outside forest (a) by elevation, and (b) compared to climate normals from WorldClim and (c) Chelsa for a network of cloud forest sites ($n = 8$, 2015–2019) and regional weather stations ($n = 32$, 1963–2019) in northern Peru. Dashed 1-to-1 lines shown in black [Colour figure can be viewed at [wileyonlinelibrary.com](https://onlinelibrary.wiley.com/terms-and-conditions)]

VPDmax decreased 0.27–0.35 kPa (Figure S5a). Global climatologies overestimated VPD at humid cloud forest sites, although there was a weak positive relationship outside forest (Figure S5b).

Across sites RHmin was significantly greater inside forest at 91% (CI 85–98) compared to 69% (CI 67–72) for weather stations outside forest ($t = 11.59$, $p < .001$). In a topographically complex region, monthly RHmin was not correlated with elevation for either cloud forest ($R_p = -0.10$, $p = .32$) or stations ($R_p = 0.03$, $p = .47$) (Figure S6a and Table S7). Monthly rainfall was weakly correlated with elevation ($R_p = -0.24$, $p < .001$) although not $>1,500$ m ($R_p = -0.12$, $p = .07$) (Figure S6b and Table S7). Change in VPD with elevation, or the VPDmax lapse rate, differed between forest and stations ($t = 2.36$, $p = .01$); the top interactive model explained 82% of the

variation (Table S9). Contrary to our prediction that VPDmax increases with warmer temperatures at lower elevation, inside humid cloud forest there was no relationship with elevation ($t = -0.41$, $p = .68$) and a VPDmax lapse rate of -0.03 kPa·km $^{-1}$ (95% CI: -0.17 to 0.11 kPa·km $^{-1}$) (Figure 8a). Conversely, our prediction was supported for stations. Outside forest a 22% reduction in RHmin resulted in a >10 -fold increase in the VPDmax lapse rate ($t = -7.87$, $p < .001$) at -0.38 kPa·km $^{-1}$ (95% CI: -0.47 to -0.28 kPa·km $^{-1}$) (Figure 8a). Drivers of VPDmax shifted from RHmin explaining 96% of the monthly variation inside forest to only 62% outside forest, whereas the explanatory power of Tmax increased from 27 to 56%.

Modelling change in monthly VPDmax by RHmin across a range of annual Tmax for all sites, reduced humidity outside forest rapidly exceeded typical water

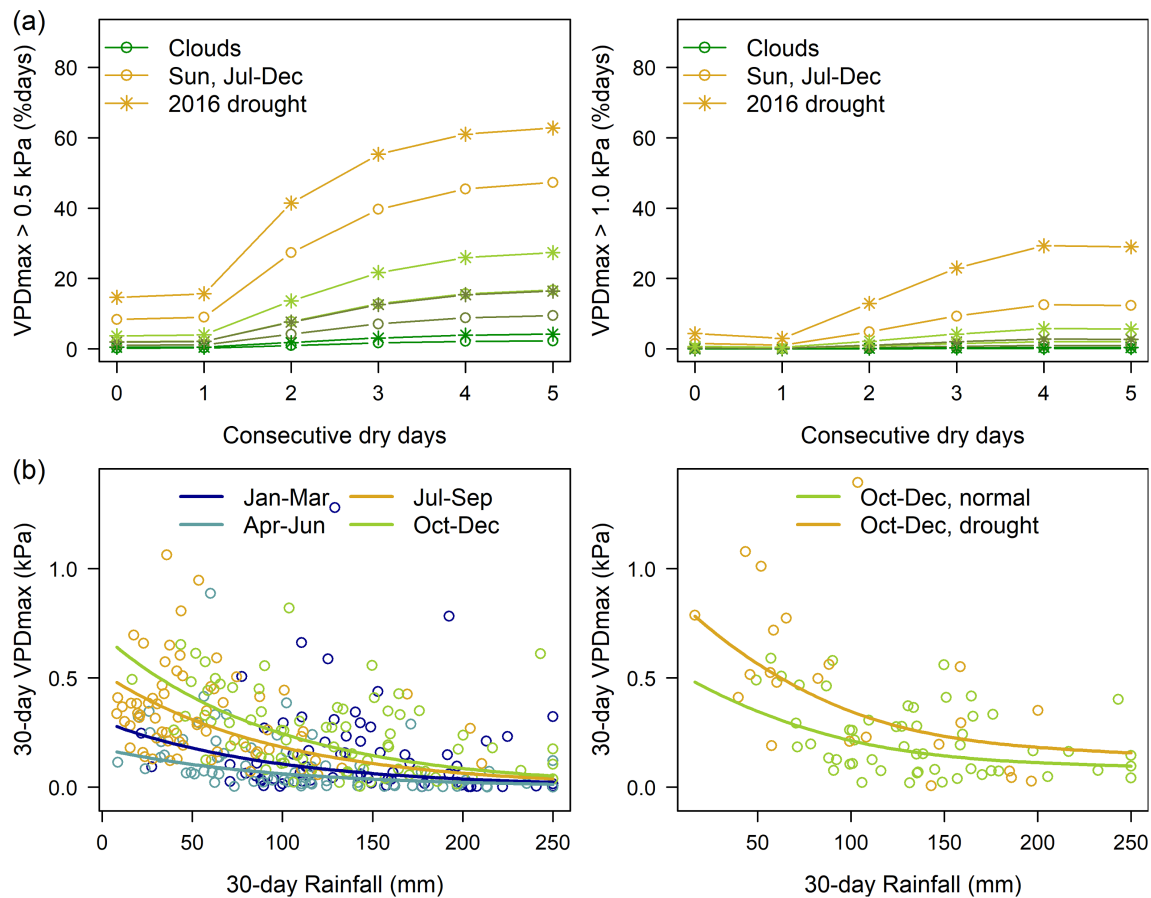


FIGURE 7 Drivers of changes in maximum vapour pressure deficit (VPDmax) or the “drying power of the air” inside cloud forest for a network of sites ($n = 8$, 2015–2019) in the Chachapoyas region of northern Peru. (a) Percent of days VPDmax exceeded thresholds each year by sun/clouds and days since rain. (b) Mean monthly VPDmax by quarter, and rainfall during normal years and an ENSO-related drought in 2016 [Colour figure can be viewed at wileyonlinelibrary.com]

stress thresholds (VPDmax >1.0 kPa) in warm tropical lowlands (Figure 8b). Above T_{max} of 27°C potential water stress occurred if RHmin fell below 80% whereas at 15°C water stress was unlikely until RHmin reached 50–60%. For a 21°C change in T_{max} across elevations, the “drying power of the air” approximately doubled per 20% reduction in humidity. At 90% RHmin mean monthly VPDmax changed <0.3 kPa, but lowland VPDmax increased 0.7 kPa at 70% RHmin, and by 50% RHmin our model predicted a 1.5 kPa increase in VPDmax indicative of substantial water stress outside forest in tropical lowlands. See Data S1 for equations explaining this pattern.

3.2 | Spatiotemporal rainfall variability in a sparse data region

3.2.1 | Latitudinal shifts in rainfall seasonality at 5° – 7°S

Across the Chachapoyas region, rainfall seasonality reflected a north-to-south latitudinal shift concurrent with

increasing seasonal temperature differentials ($\sim 0.8^{\circ}\text{C}$). At cloud forest sites, rainfall peaked 3 weeks earlier south of 6°S along with a 41% reduction in minimum dry-season rainfall initiating water stress (32 vs. 54 $\text{mm}\cdot\text{month}^{-1}$) (Figure 9a). Weather stations reflected similar reductions in May–September rainfall south of 6°S , although shifts in timing were less clear (Figure 9d). For our network of sites southeast of the Marañon River, daytime rain was more seasonal than night-time rain with greater nocturnal dry season rain north of 6°S (Figure 9b). Rain primarily occurred during late morning or afternoon except for October–December when rain occurred at any time of day (Figure S1); limited data from the eastern slopes suggest reduced diurnal rain cycles. Northwest of the Marañon River, weather stations were generally characterized by greater nocturnal rain indicating greater downslope instead of upslope wind flow (Figure 9c). Models of long-term rainfall seasonality show our network of cloud forest sites bordered on water stress thresholds around 50 $\text{mm}\cdot\text{month}^{-1}$ during the driest months, except for the eastern slopes, but exceeded >150 $\text{mm}\cdot\text{month}^{-1}$ during the wettest months (Figure 10).

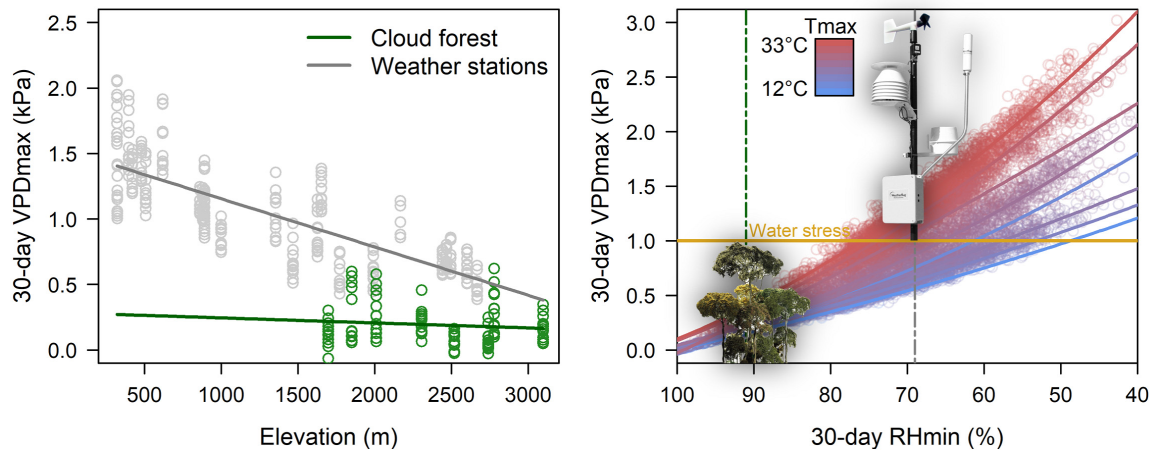


FIGURE 8 Buffering effect of humid forest microclimate on maximum vapour pressure deficit (VPD_{max}) or the “drying power of the air.” (a) Partial regression for monthly normals by elevation inside versus outside forest. (b) Feedback whereby temperature magnified VPD_{max} as minimum relative humidity (RH_{min}) decreased. Dashed lines show mean RH_{min} inside versus outside forest relative to typical water stress thresholds (VPD_{max} > 1 kPa). Data points represent monthly means by site and year for cloud forest ($n = 8$, 2015–2019) and regional weather stations ($n = 31$, 1963–2019) in northern Peru [Colour figure can be viewed at [wileyonlinelibrary.com](https://onlinelibrary.wiley.com/doi/10.1002/joc.7567)]

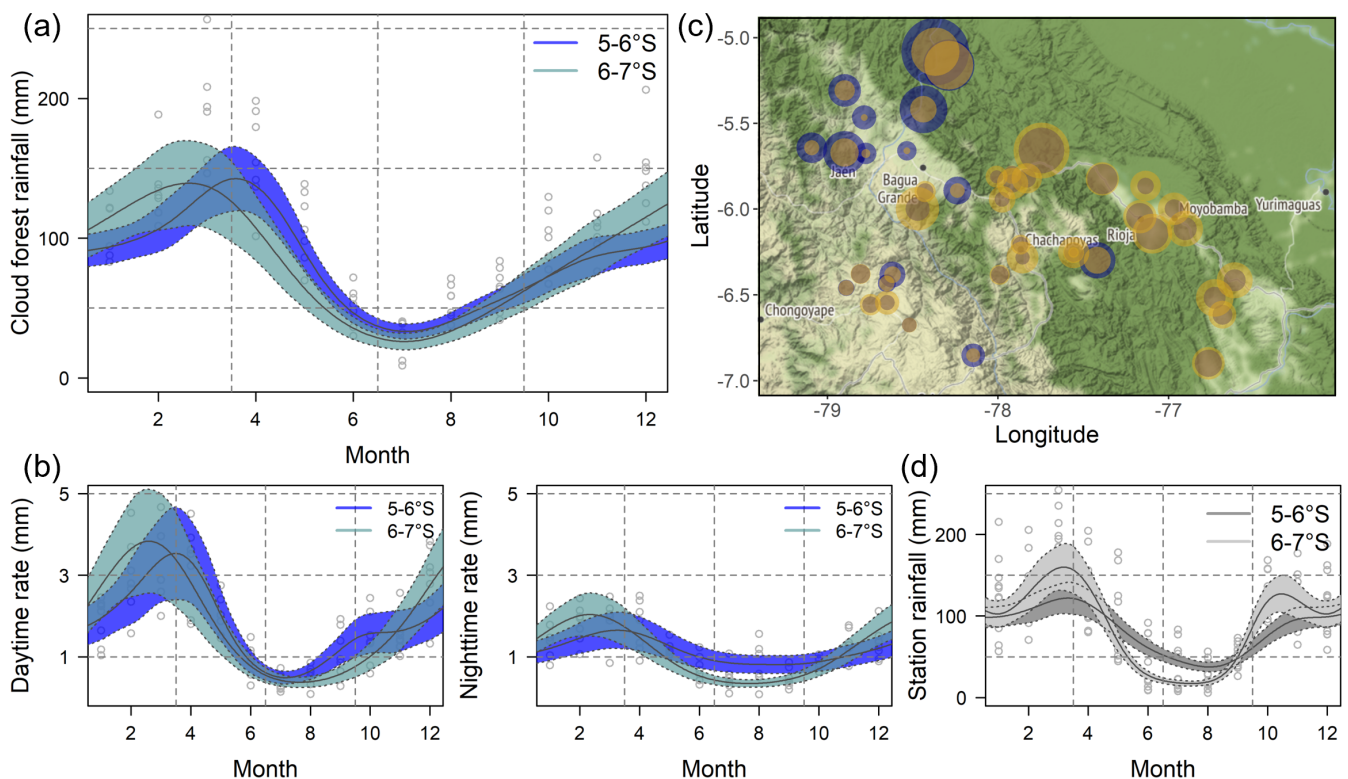


FIGURE 9 Seasonal shift in rainfall by latitude. (a) Mean monthly rainfall and (b) diurnal/nocturnal rain rate ($\text{mm}\cdot 12 \text{ hr}^{-1}$) across a network of cloud forest sites ($n = 8$, 2015–2019). (c) Mean diurnal/nocturnal rain rate across the region and (d) seasonal shift in mean monthly rainfall for regional weather stations within 100 km ($n = 46$, 1963–2019) [Colour figure can be viewed at [wileyonlinelibrary.com](https://onlinelibrary.wiley.com/doi/10.1002/joc.7567)]

3.2.2 | Local rainfall compared to gridded climatologies in a sparse data region

In a sparse data region gridded precipitation remained imprecise compared to temperature, explaining <50% of

the variation (Figures 11 and S4). Based on centred intercepts (Table S10), gridded datasets predicted moderate rainfall ($\leq 150 \text{ mm}\cdot \text{month}^{-1}$) within 5–13 $\text{mm}\cdot \text{month}^{-1}$ (MAE 20–24) except for GPM IMERG which consistently overestimated moderate rainfall by 31 $\text{mm}\cdot \text{month}^{-1}$

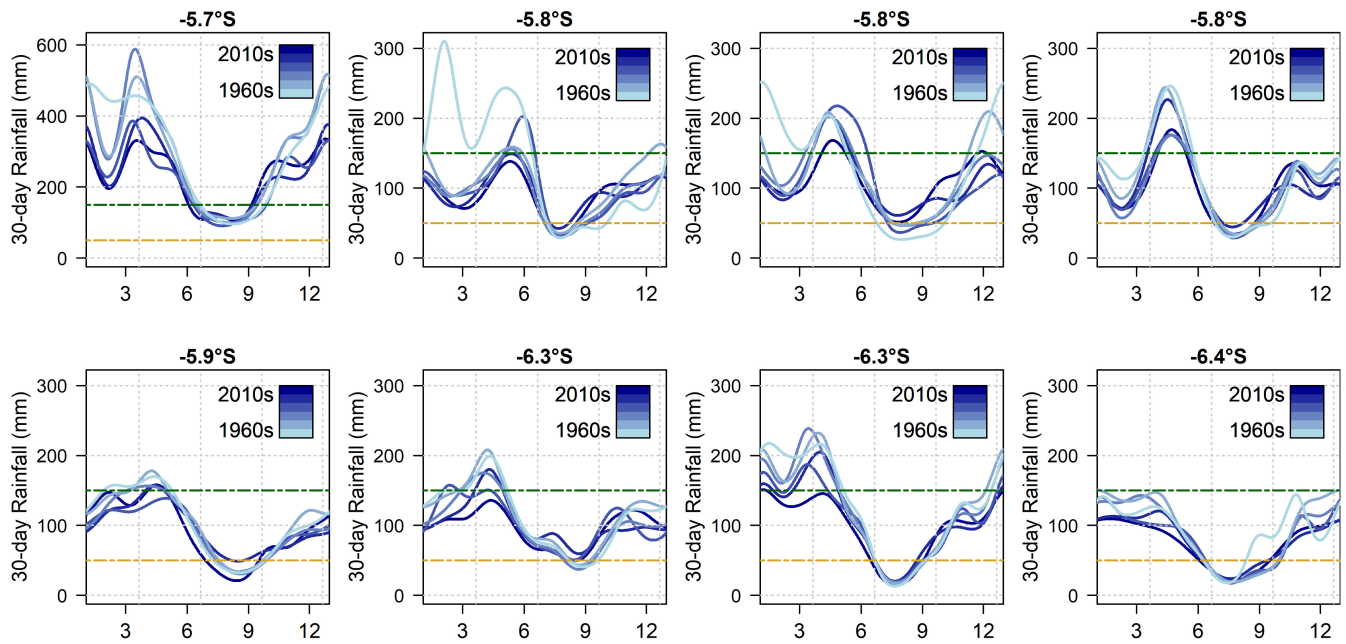


FIGURE 10 Models for seasonal rainfall by decade since the 1960s at a network of cloud forest sites in the Chachapoyas region of northern Peru. Models integrate a short-term network of rain gauges and long-term weather stations to describe spatiotemporal variation scaled to cloud forest. Dashed lines indicate approximate water stress thresholds ($<50 \text{ mm}\cdot\text{month}^{-1}$) and heavy rain ($>150 \text{ mm}\cdot\text{month}^{-1}$) [Colour figure can be viewed at wileyonlinelibrary.com]

(MAE 37). WorldClim overestimated the driest months (zero-intercept $23\text{--}26 \text{ mm}\cdot\text{month}^{-1}$) but underestimated rainfall $>80 \text{ mm}\cdot\text{month}^{-1}$ (1:1 ratio 0.58–0.63). Chelsa v2.1 was the only dataset to overestimate moderate cloud forest rainfall by $29 \text{ mm}\cdot\text{month}^{-1}$ (CI 9–49), although station rainfall was within $4 \text{ mm}\cdot\text{month}^{-1}$ (CI –6 to 14). CHIRPS and related PISCO increased linearly with observed rainfall (1:1 ratio 0.93–0.94), but all gridded datasets underestimated heavy rainfall ($>150 \text{ mm}\cdot\text{month}^{-1}$) by 31–80 $\text{mm}\cdot\text{month}^{-1}$ (MAE 60–84) except for GPM IMERG which was within $4 \text{ mm}\cdot\text{month}^{-1}$ despite variability (MAE 54). Missing heavy rainfall contributed to gridded datasets predicting annual rainfall $>1,000 \text{ mm}$ poorly (Figure 11b) although all datasets partially captured seasonal rainfall shifts across the region (Figure S5).

3.3 | Interannual variability and regional trends compared to CHIRPS

During a 5-year period, we captured interannual variability around a strong El Niño event in 2015–2016. Despite regional warming of 1°C through the first quarter of 2016 (T_{min} , T_{max}), after Pacific Ocean warming dissipated by June, T_{min} dropped 0.5°C in October–December at cloud forest and montane stations, but not below 1,300 m

(Figure 12). At the same time T_{max} , after returning near normal from April–September, increased 1.5°C region-wide from October to December along with concurrent 10% decreases in cloud cover, 5–10% decreases in RH_{min} and a 0.2 kPa increase in VPD_{max}. Drought was most apparent at cloud forest sites where daily rain rates were reduced $>1.5 \text{ mm}\cdot\text{day}^{-1}$ while RH_{min} fell $>8\%$ (Figure 12). A 20% reduction in regional rainfall in October–December 2016 was apparent in the three gridded datasets we examined: CHIRPS, GPM-IMERG, and PISCO (Figure S8), and cloud forest sites toward the eastern slopes showed the greatest rainfall reductions (Figure S12).

Over 50 years temperature and rainfall increased in northern Peru (Figure S10), but trends varied seasonally (Figure 13) and by metric (Figure S11). T_{min} increased in all seasons at $+0.16\text{--}0.23^\circ\text{C}\cdot\text{decade}^{-1}$ (CI 0.06–0.33), whereas T_{max} varied by season, with greatest increases during the dry season at $+0.25^\circ\text{C}\cdot\text{decade}^{-1}$ (CI 0.12–0.38), weaker increases during the transition wet season at $+0.13^\circ\text{C}\cdot\text{decade}^{-1}$ (CI 0.07–0.20), but no change from January–June (CI –0.11 to 0.12). Changes in VPD_{max} reflected seasonal change in RH_{min} with increasingly humid wet seasons (VPD_{max} $-0.02 \text{ kPa}\cdot\text{decade}^{-1}$ CI –0.04 to –0.01, RH_{min} $+0.6\%$ decade^{-1} CI 0.2–0.9), whereas humidity was reduced during the dry season (VPD_{max} $+0.02 \text{ kPa}\cdot\text{decade}^{-1}$ CI 0.01–0.04, RH_{min} -0.5% decade^{-1} CI –0.9 to –0.1), while transitional seasons did not change (VPD_{max} CI –0.01 to

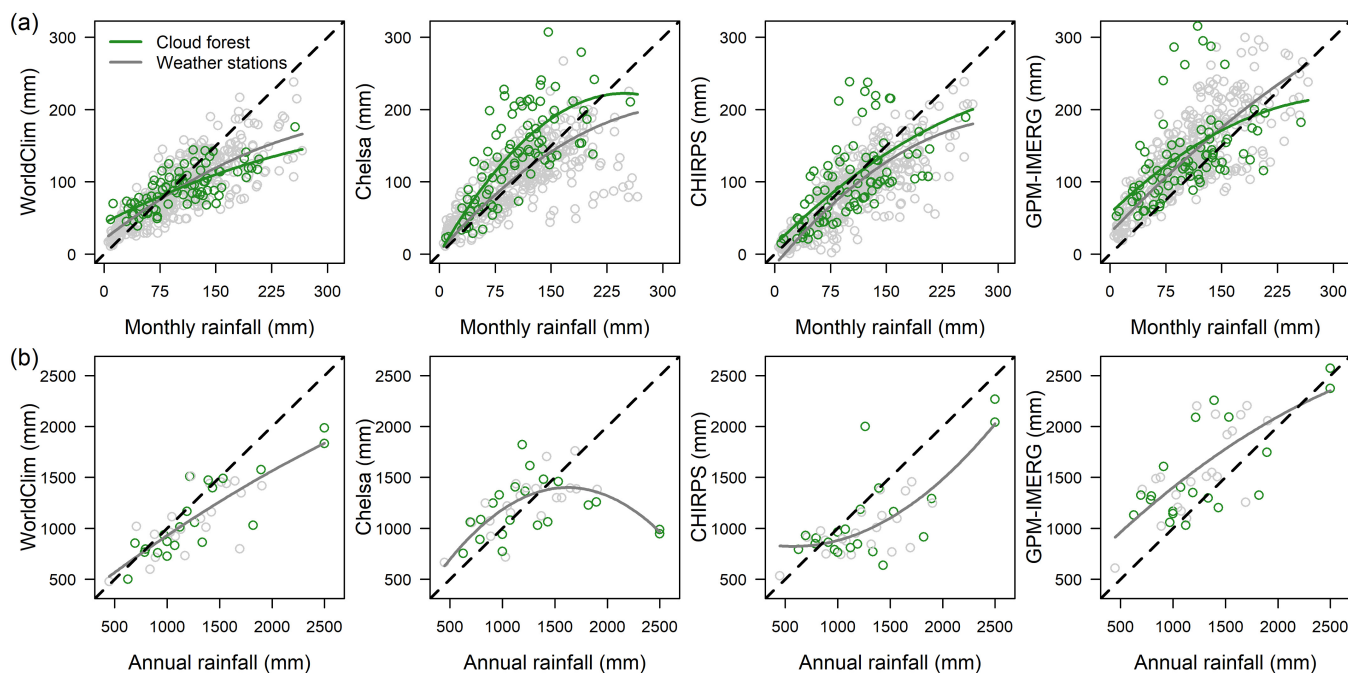


FIGURE 11 Gridded climatologies compared to in situ data. (a) Mean monthly and (b) mean annual rainfall from WorldClim, Chelsa, CHIRPS, and GPM-IMERG compared to rain gauges for a network of cloud forest sites ($n = 8$, 2015–2019) and regional weather stations ($n = 46$, 1963–2019) in northern Peru. Dashed 1-to-1 lines shown in black [Colour figure can be viewed at [wileyonlinelibrary.com](https://onlinelibrary.wiley.com/doi/10.1002/joc.7567)]

$0.02 \text{ kPa}\cdot\text{decade}^{-1}$, RHmin CI -0.65 to $0.32\%\cdot\text{decade}^{-1}$). Precipitation increased $+5\text{--}6\%\cdot\text{decade}^{-1}$ (CI 4–8) during the wet and transition wet seasons but decreased $-4\%\cdot\text{decade}^{-1}$ (CI -2 to -6) during the dry season with no change during the transition to the dry season (Figure 13).

Trend analysis for both the normal ratio method (NRM) and CHIRPS predicted decadal increases in wet-season rainfall at cloud forest sites with high certainty (Figure 14), although at $+8\text{--}10\%\cdot\text{decade}^{-1}$ CHIRPS predicted greater magnitude increases than NRM models. Increasing rainfall was found for all analytical approaches, but weak decreases in dry-season rainfall were only apparent with Gamma regression for long-term stations (Figure S12). NRM models predicted a similar pattern at cloud forest sites (Figure 14) primarily driven by a decrease in dry-season rainfall variability and increasingly regular dry seasons with reduced occurrence of year-round rain at most long-term stations (Figure 11b). A weaker trend, decreasing dry-season variability was not detected by CHIRPS or Sen's slope with additional long-term data needed to confirm this pattern.

Reflecting response to complex topography we also found evidence for local variation in trends. Decadal trends for 22 long-term stations showed the greatest warming at northern sites with greatest reductions in dry season rainfall at southern sites $>1,300 \text{ m}$, including the city of Chachapoyas (Figures S11 and S12). Across the region increasing rainfall in January–February was especially evident for northeastern cloud forest sites

(Figure S12). At cloud forest sites NRM models reflected decreasing dry-season rainfall for the Chachapoyas region at $-4\%\cdot\text{decade}^{-1}$ (Figure 13) while analysis of seasonal drought indicated the strongest droughts occurred during the 1980s (Figure S11). Interannual variability in temperature related to Pacific Sea surface temperatures with strongest correlations with the Oceanic Niño Index (ONI) whereas rainfall related to pressure correlated with both the Equatorial Southern (EQSOI) and Antarctic (AAO) oscillations (Tables S12–S15).

4 | DISCUSSION

4.1 | Microclimatic buffering effect of forests

4.1.1 | Temperatures inside versus outside forest compared to gridded climatologies

Our results are consistent with strong buffering effects of forest which reduce climatic extremes in the understory (Davis *et al.*, 2019; De Frenne *et al.*, 2021). Reducing diurnal amplitude, we found around 4°C reductions in maximum and 1°C increases in minimum temperatures inside compared to outside forest, magnitudes surprisingly close to both global meta-analysis (De Frenne *et al.*, 2019) and satellite data across the tropics, although satellites did

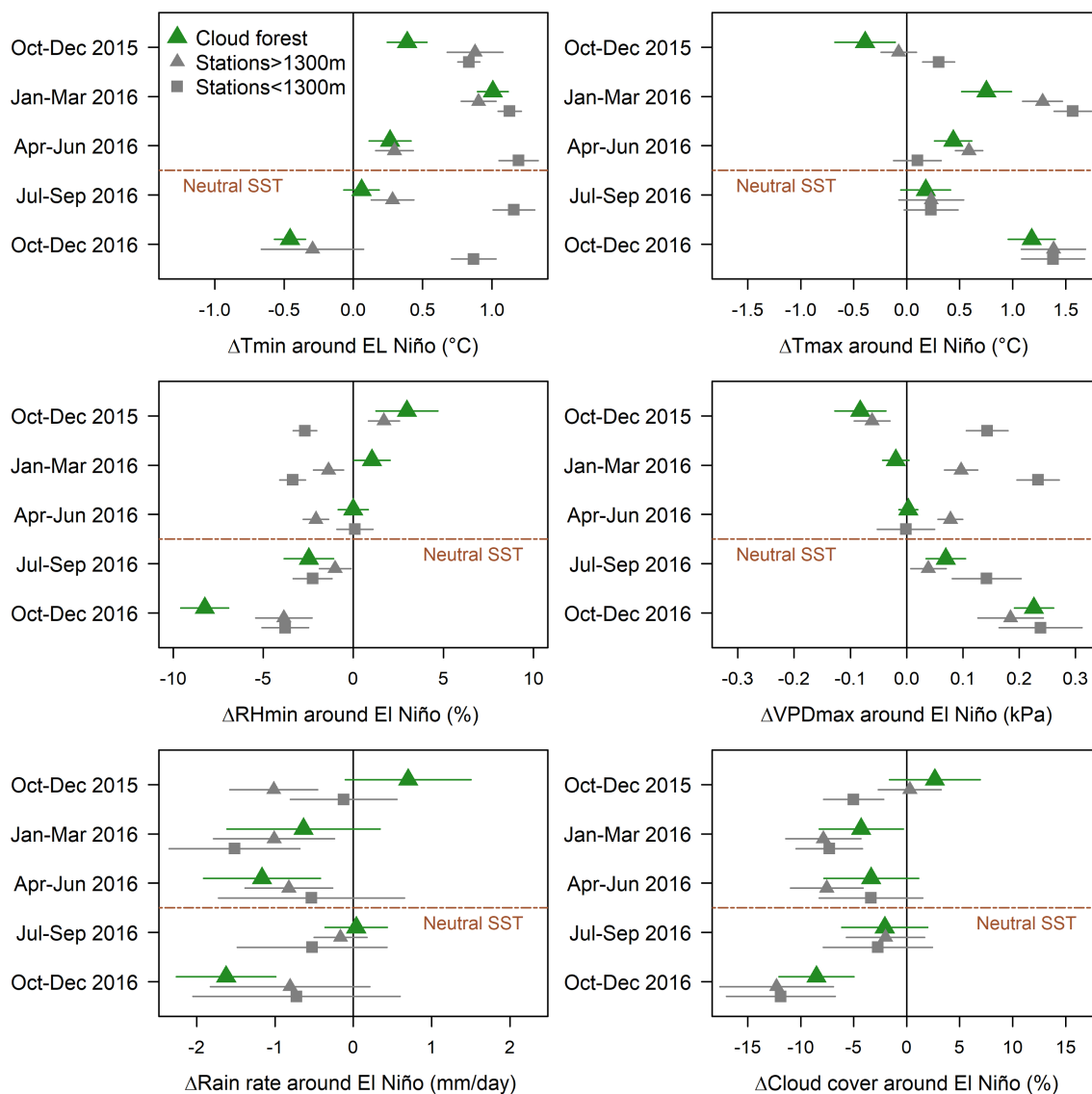


FIGURE 12 Seasonal change in temperature, relative humidity (RH), vapour pressure deficit (VPD), rain rate, and cloud cover around the 2015–16 El Niño compared to normal years for a network of cloud forest sites ($n = 8$, 2015–2019) and regional weather stations by elevation ($n = 11$ –13) in northern Peru. Error bars represent 95% confidence intervals from daily analysis. Dashed line shows dissipation of El Niño conditions and return to neutral sea surface temperatures (SST) [Colour figure can be viewed at [wileyonlinelibrary.com](https://onlinelibrary.wiley.com/terms-and-conditions)]

not detect warmer night-time temperatures (Li *et al.*, 2015). Foliage cover is a strong predictor of vegetative cooling (Hardwick *et al.*, 2015; Jucker *et al.*, 2018; Davis *et al.*, 2019). Despite using weather stations as a broad proxy for outside forest, our results are consistent with global analysis of land-use change showing forest loss amplifies diurnal temperature variation, and increases mean and maximum temperatures (Alkama and Cescatti, 2016).

Reflecting moisture recycled by trees, we found forest loggers predicted a more humid near-surface lapse rate than regional weather stations, especially for maximum air temperatures. Compared with published microclimate data along the eastern slopes of the Andes, our drier

Tmax lapse rates in Sept matched seasonal Tmean lapse rates in the Manu at 13°S (Rapp and Silman, 2012), whereas Tmin matched limited seasonality at Estación Científica San Francisco at 3°S, although nearby pasture lapse rates dropped in Sept (Fries *et al.*, 2009). Station lapse rates in southern Peru are generally more seasonal (Navarro-Serrano *et al.*, 2020) as relative humidity changes with latitude (Peixoto and Oort, 1996).

Global climatologies differed in their ability to reflect cloud forest microclimate, primarily cooler maximum temperatures inside forest. Using different interpolation versus statistical downscaling approaches, on average WorldClim was within 1°C outside forest whereas Chelsea was within 1°C inside forest, an improvement for forest

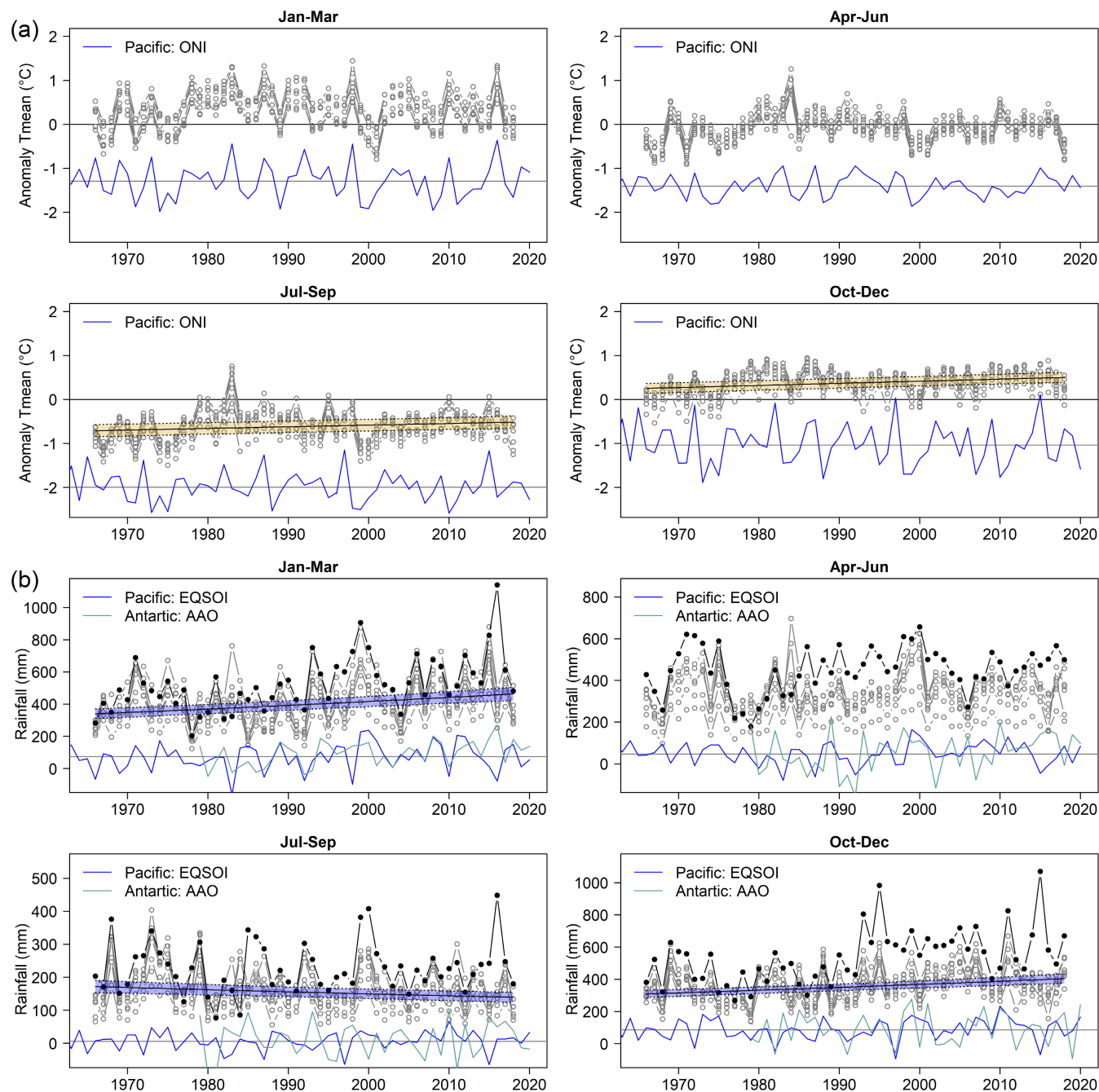
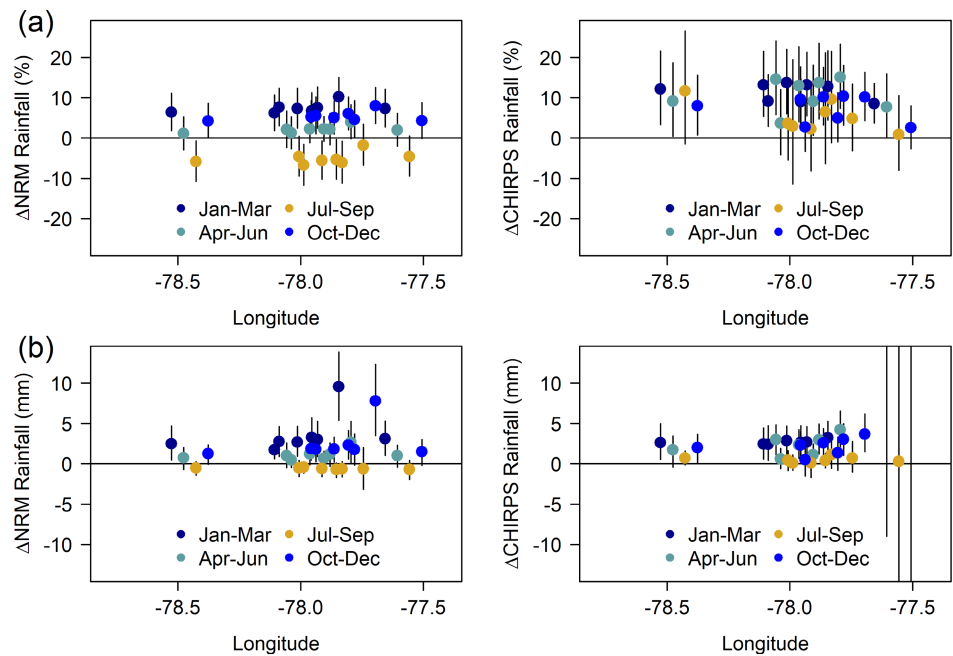


FIGURE 13 Interannual variability and trends by season for (a) mean quarterly temperature anomalies and (b) quarterly rainfall accumulation in the Chachapoyas region of northern Peru. Temperature and rainfall scaled to cloud forest sites using the normal ratio method. Significant trends ($p < .05$), and global teleconnections with the strongest correlation by season included on each graph [Colour figure can be viewed at [wileyonlinelibrary.com](https://onlinelibrary.wiley.com/doi/10.1002/joc.7567)]

biodiversity studies. WorldClim also overestimated maximum temperatures in tropical rainforest (Jucker *et al.*, 2018) whereas Chelsa underestimated mean temperatures at Colombian weather stations (Bastidas Osejo *et al.*, 2019). Our results inform choice of gridded datasets for different applications. Climate datasets that best reflect species ecology can improve distributional

modelling (Lembrechts *et al.*, 2019) and with a growing understanding of the buffering effects of forest microclimate, gridded climatologies are needed that explicitly model forest versus open land for different applications. Despite high temperature predictability, our forest microclimate data demonstrate current challenges to modelling fine-scale near-surface water vapour.

FIGURE 14 Decadal change in rainfall by season at cloud forest sites from the normal ratio method (NRM) compared to CHIRPS in the Chachapoyas region of northern Peru. (a) Coefficients from Gamma regression and (b) Sen's slope; error bars represent 95% confidence intervals [Colour figure can be viewed at wileyonlinelibrary.com]



4.1.2 | Forest humidity buffers warming-induced drying across elevations

Using in situ data, we show interactions between climate and land-use across a complex 1,400-m elevational gradient decorelated with relative humidity. Weather stations matched our original prediction that VPD increases at warmer lower elevations, whereas cloud forests maintained low VPD in the understory. Inside rainforest, VPD was also relatively constant across a 200–700 m gradient in Borneo (Jucker *et al.*, 2018) suggesting the phenomenon we observed is not restricted to cloud forest. At higher latitude in southern Peru and Costa Rica, forest VPD decreased with elevation along with concurrent changes in precipitation and cloud cover (Rapp and Silman, 2012; Gotsch *et al.*, 2017). Covariance between temperature and moisture is a common problem on elevational gradients (Körner, 2007), and our system spanning four watersheds provides unique insight by isolating temperature.

Effects of forest microclimate on warming-induced evaporative drying reflect the dominate role of trees in terrestrial water fluxes. Near-surface atmospheric water balance and VPD are tightly linked to plant transpiration (Jasechko *et al.*, 2013) although forests can also influence surface albedo and aerodynamic roughness (Pielke *et al.*, 2007). Evaporation increases with warming whereas plant physiology regulates transpiration. Our results suggest that with normal rainfall, humid forests can stabilize warming-induced drying across elevations, perhaps because transpiration typically increases with VPD up to a given threshold (Grossiord *et al.*, 2020). Forest buffering of VPD and maximum temperature can change with soil

water balance (Davis *et al.*, 2019) and we found forest VPD increased after the 2016 El Niño when rainfall was reduced during peak solar insolation. Further work is needed to examine if warmer temperatures at lower elevation magnify drought. Additionally, how our results relate to forest function remains unclear. Forests also represent vertical microclimate gradients (Davis *et al.*, 2019) with decreasing canopy humidity (Rapp and Silman, 2012; Nakamura *et al.*, 2017) as transpiration forms a rising column of humid air (Makarieva and Gorshkov, 2007; Sheil, 2018). Humid forests provide important regulatory services recycling rainfall (Spracklen *et al.*, 2012; 2018), although in arid systems non-native trees can reduce water tables (Schwärzel *et al.*, 2020). Amazon rainforests buffer against drought (Staal *et al.*, 2018) and deforestation has been shown to delay start of the rainy season (Butt *et al.*, 2011; Leite-Filho *et al.*, 2019), reduce regional rainfall by as much as 40% (Spracklen *et al.*, 2012; 2018), and link to drying of the lower atmosphere contributing to wildfires (Xu *et al.*, 2020). Globally, forests maintain dry season transpiration by accessing soil moisture through deep roots reducing downwind precipitation variability (O'Connor *et al.*, 2021).

4.2 | Spatiotemporal rainfall variability in a sparse data region

4.2.1 | Latitudinal shifts in rainfall seasonality at 5°–7°S

Our results demonstrate a seasonal shift in rainfall around 6°S. North of this latitude the peak of the rainy

season was 3 weeks later with rainfall on average >50 mm·month⁻¹ year-round. Wetter dry seasons were driven by greater nocturnal rain while diurnal rain was more seasonal. Subtle seasonal shifts in timing and extent of rainfall are consistent with a transition zone between the Northern and Central Andes (Segura *et al.*, 2019). Related to the southernmost extent of the Intertropical Convergence Zone (ITCZ), rainfall seasonality north of 6°S matched the equatorial Andes with peaks from February to April, and the driest months July–September (Segura *et al.*, 2019). To the south seasons are shifted a month earlier with the dry season June–August and heaviest rainfall December–February related to the mature phase of the South American monsoon system (Segura *et al.*, 2019).

Convergence of different weather patterns may contribute to several rainfall peaks (Knoben *et al.*, 2019). In the transition zone around Chachapoyas, a weak rainfall peak in October–November has been related to increased convection over the equatorial Amazon while a second larger peak in February–April may be caused by intensification of the eastern branch of the Walker Cell and southward migration of the ITCZ (Segura *et al.*, 2019). Our data show January–February rainfall was reduced in some years, especially at northern sites during El Niño conditions in 2016 and 2019, although this region does not experience consistently alternating wet and dry seasons. Truly bimodal rainfall has only been recorded for 7.9% of the tropics including northern South America and Central Africa (Knoben *et al.*, 2019).

Our limited data document greatest rainfall on the eastern slopes consistent with prevailing winds from the Amazon basin which turn south to form the South American Low-Level Jet (SALLJ) (Figure 2a). Heaviest rainfall generally occurs on the first ridge of the Andes, and in premontane forest in Ecuador, stations commonly report 6,000 mm·year⁻¹ on the eastern slopes (Laraque *et al.*, 2007) while along the length of the Andes TRMM satellite data show rainfall peaks between 1,000 and 1,300 m (Laraque *et al.*, 2007; Bookhagen and Strecker, 2008; Chavez and Takahashi, 2017). At the lowest point of the Andes around the Marañón River Valley, northern Peru is often considered a “dry spot” (Killeen *et al.*, 2007) with extreme rainfall events ≤ 100 mm·day⁻¹, although 2× this may fall during a day in southern Peru (Domínguez-Castro *et al.*, 2018; Rodríguez-Morata *et al.*, 2018). Although rainfall magnitude remains unclear, our data support field observations that less accessible northeastern facing slopes in Bosque de Protección Alto Mayo and the Cordillera de Colán receive extensive rainfall (L.G. Rimarachín Cayatopa, A. García Bravo, BPAM park guards, personal communication).

Regional shifts in timing and magnitude of rainfall may have influenced early human settlement patterns in the Andes. The city of Chachapoyas, capital of the

department of Amazonas, is named after the pre-Incan culture which occupied the region between the Marañón and Huallaga rivers from 800 to 1,500 AD. Interestingly, population centres of the Chachapoyas culture appear to have been primarily located in drier areas south of the seasonal rainfall shifts that we documented, as well as west of the eastern slopes. Two of the larger ruins in Amazonas, Yalape and Kuelap, are situated near where we documented reduced dry-season rainfall. Perhaps stronger dry seasons made burning and clearing land easier. During past dry periods, lake pollen cores indicate increased cultivation of less humid crops such as maize to the north around the town of Pomacochas (Åkesson *et al.*, 2020) where we show dry seasons today are generally less pronounced. This suggests human populations could have extended northward to take advantage of drier conditions, whereas today Pomacochas is a centre of dairy production.

4.2.2 | Local rainfall compared to gridded climatologies in a sparse data region

Gridded precipitation remains especially limited by station density in remote low-latitude mountains. Datasets we examined reflected regional rainfall seasonality with a coarse approximation of latitudinal shifts. CHIRPS provided the best estimate of rainfall magnitude both inside and outside forest, increasing linearly with observed values and explaining around half the variation for in situ rain gauges. Other studies have found CHIRPS to be the best option in tropical regions (Beck *et al.*, 2017), although WorldClim and Chelsa explained $>70\%$ of the variation for higher density stations in Brazil and Colombia (Bastidas Osejo *et al.*, 2019; de Oliveira-Júnior *et al.*, 2021). In northern Peru, CHIRPS predicted rainfall greater than 150 mm·month⁻¹ and 1,000 mm·year⁻¹ poorly. Satellite-based datasets typically underestimate montane rainfall (Beck *et al.*, 2020), although streamflow bias corrections (Beck *et al.*, 2020) in Chelsa v2.1 overestimated rainfall for our cloud forest network, perhaps because source allocation becomes problematic in a topographically complex region. CHIRPS also reflected only coarse resolution spatiotemporal variability at local scales. This was especially problematic on the eastern slopes where we documented nearly 3× the CHIRPS estimate in 2015–2016, while CHIRPS overestimated rainfall at a second site near the eastern slopes.

In the Chachapoyas region weather stations are primarily located in drier populated areas, and our results demonstrate the importance of a network of gauges to capture fine-scale topographic complexity. Above the inflection point for orographic rainfall (Bookhagen and Strecker, 2008), mountains are often characterized by a

constant, but relatively low rate of rain or drizzle (Rollenbeck and Bendix, 2011) with annual rainfall generally <3,000 mm and weather stations commonly reporting 500–1,500 mm·year⁻¹ as in our study (Laraque *et al.*, 2007; Espinoza Villar *et al.*, 2009). We found generally drier conditions were more accurate, and drier valleys often form predictably from rain shadow effects on western or southern facing slopes of high mountains in this region, as well as along narrow canyons where clouds pass over warm rising air without precipitating (Killeen *et al.*, 2007). Wetter sites can receive nocturnal drainage from higher terrain with maximum rainfall in the early morning whereas afternoon rainfall may be common at drier sites (Junquas *et al.*, 2018).

4.3 | Interannual variability and regional trends compared to CHIRPS

Five years of data collection included a strong El Niño event in 2015–2016 which especially impacted the wet tropics (Rifai 2019). In northern Peru a combination of reduced rainfall and increased evaporative demand contributed to region-wide drought in the austral spring, several months after El Niño conditions dissipated. Drought may have related to phase of Arctic Oscillation which is currently correlated with the North Atlantic Oscillation influencing rainfall across Peru (Mohammadi *et al.*, 2020). Reduced rainfall and humidity were especially apparent in cloud forest as daytime temperatures increased and nighttime temperatures dropped. In November 2016 wildfires burned some of the last remaining relic cloud forests on the western slopes of the Andes in northern Peru (Mutke *et al.*, 2017) providing a warning for the future if droughts occur regularly. In the Chachapoyas region, burning is believed to induce rain leading to increased use of fire when forests are most at risk. Rain gauge data since the 1960s suggest more regular dry seasons with reduced occurrence of year-round rain combined with increasing evaporative demand. Modelling shows a 10× increase in extinction risk from changing rainfall (McCain and Colwell, 2011) while some evidence suggests ecotonal limits of cloud forest may be structured by extreme ENSO events (Crausbay *et al.*, 2014).

At the same time as documenting drought, we found strong support for regional increases in wet season rainfall consistent with other studies (Urrutia and Vuille, 2009; Rascón *et al.*, 2021). Over the past 50 years we estimated wet season rainfall increased ~40% region-wide, with concurrent increases in T_{min} of ~1°C. Extreme rainfall events can contribute to flooding and landslides, especially in mountainous regions (Poveda *et al.*, 2020). Although the major paved east–west road

from Chiclayo to Tarapoto crosses at the low point of the Andes, transportation regularly shuts down in March and April, isolating mountain cities such as Chachapoyas. In April 2016 >40 mm of rain fell in a few hours washing out the hydroelectric plant for the town of Beruit in the district of Corosha, resulting in permanent loss of community infrastructure.

In the absence of alterations to global atmosphere and ocean circulation, the Chachapoyas region of northern Peru is likely to experience greater seasonal extremes of both flooding and drought consistent with amplification of precipitation variability in wet regions (Zhang *et al.*, 2021). Ongoing deforestation is likely to exacerbate extremes (Ellison *et al.*, 2017; Chapman *et al.*, 2020). Gridded datasets provide a useful tool to integrate across space and time, but we demonstrate the utility of in situ data to capture both forest microclimate and fine-scale variation in rainfall. Our results highlight the importance of developing long-term climate monitoring in remote biodiverse regions across the Andes, including change in forest microclimate (Zellweger *et al.*, 2020).

AUTHOR CONTRIBUTIONS

Felicity L. Newell: Conceptualization; data curation; formal analysis; funding acquisition; investigation; methodology; project administration; validation; visualization; writing – original draft; writing – review & editing. **Ian J. Ausprey:** Methodology; project administration; visualization; writing – review and editing. **Scott K. Robinson:** Funding acquisition; resources; supervision; writing – review and editing.

ACKNOWLEDGEMENTS

We thank the following funding sources: IDEA Wild, Katharine Ordway Chair of Ecosystem Conservation at the Florida Museum of Natural History, and University of Florida Department of Biology Grinter and CLAS Dissertation fellowships to FLN. We especially thank landowners and families in Peru who supported collection of weather data on their property including H. Francisco Lopez, M. Llaja; D. Poclín Pinedo, D. Poclín Tuesta, E. Díaz Guamuro, V. Chavez and family, L.G. and V.R. Rimarachín Cayatopa, R. Rimarachín, C. Cayatopa, P. Mori Cachay, M. Servan Cruz, D.C and P. Mori Servan, H. and S. Vilca, J. La Torre, A. Cuipal Chuquisuta, A. Chavez, Y. Paico and BPAM park guards. We thank W.G. Castillo, P. Heredia Arce, and Universidad Toribio Rodríguez de Mendoza INDES-CES, especially R. Salas López and E. Barboza, for contributing additional weather data for Amazonas. We thank J. Lichstein and B. Loiselle for starting us thinking about VPD and evaluating climatologies. The manuscript was improved by comments from two anonymous reviewers. Open Access

Funding provided by Universitat Bern. [Correction added on 20 May 2022, after first online publication: CSAL funding statement has been added.]

DATA AVAILABILITY STATEMENT

Data are available at figshare <https://doi.org/10.6084/m9.figshare.18543167> (Newell *et al.*, 2022).

ORCID

Felicity L. Newell  <https://orcid.org/0000-0002-7944-8603>

Ian J. Ausprey  <https://orcid.org/0000-0002-7127-2746>

REFERENCES

- Abatzoglou, J.T., Dobrowski, S.Z., Parks, S.A. and Hegewisch, K.C. (2018a) TerraClimate, a high-resolution global dataset of monthly climate and climatic water balance from 1958–2015. *Scientific Data*, 5, 170191. <https://doi.org/10.1038/sdata.2017.191>.
- Abatzoglou, J.T., Williams, A.P., Boschetti, L., Zubkova, M. and Kolden, C.A. (2018b) Global patterns of interannual climate–fire relationships. *Global Change Biology*, 24, 5164–5175. <https://doi.org/10.1111/gcb.14405>.
- Åkesson, C.M., Matthews-Bird, F., Bitting, M., Fennell, C.-J., Church, W.B., Peterson, L.C., Valencia, B.G. and Bush, M.B. (2020) 2,100 years of human adaptation to climate change in the High Andes. *Nature Ecology & Evolution*, 4, 66–74. <https://doi.org/10.1038/s41559-019-1056-2>.
- Alkama, R. and Cescatti, A. (2016) Biophysical climate impacts of recent changes in global forest cover. *Science*, 351, 600–604. <https://doi.org/10.1126/science.aac8083>.
- Anderson, C.I. (2018) senamhiR: a collection of functions to obtain Peruvian climate data. R package version 0.7.0. <https://gitlab.com/ConorIA/senamhiR/>
- Anderson, D.B. (1936) Relative humidity or vapor pressure deficit. *Ecology*, 17(2), 277–282. <http://doi.org/10.2307/1931468>
- Ault, T.R. (2020) On the essentials of drought in a changing climate. *Science*, 368, 256–260. <https://doi.org/10.1126/science.aaz5492>.
- Ausprey, I.J., Newell, F.L. and Robinson, S.K. (2020) Adaptations to light predict the foraging niche and disassembly of avian communities in tropical countrysides. *Ecology*, 102, e03213. <https://doi.org/10.1002/ecy.3213>.
- Aybar, C., Fernández, C., Huerta, A., Lavado, W., Vega, F. and Felipe-Obando, O. (2020) Construction of a high-resolution gridded rainfall dataset for Peru from 1981 to the present day. *Hydrological Sciences Journal*, 65, 770–785. <https://doi.org/10.1080/02626667.2019.1649411>.
- Bastidas Osejo, B., Betancur Vargas, T. and Alejandro Martinez, J. (2019) Spatial distribution of precipitation and evapotranspiration estimates from Worldclim and Chelsea datasets: Improving long-term water balance at the watershed-scale in the Urabá region of Colombia. *International Journal of Sustainable Development and Planning*, 14, 105–117. <https://doi.org/10.2495/SDP-V14-N2-105-117>.
- Bates, D., Mächler, M., Bolker, B. and Walker, S. (2015) Fitting linear mixed-effects models using lme4. *Journal of Statistical Software*, 67, 1–48. <https://doi.org/10.18637/jss.v067.i01>.
- Beck, H.E., Vergopolan, N., Pan, M., Levizzani, V., van Dijk, A.I.J.M., Weedon, G.P., Brocca, L., Pappenberger, F., Huffman, G.J. and Wood, E.F. (2017) Global-scale evaluation of 22 precipitation datasets using gauge observations and hydrological modeling. *Hydrology and Earth System Sciences*, 21(12), 6201–6217. <http://doi.org/10.5194/hess-21-6201-2017>
- Beck, H.E., Wood, E.F., McVicar, T.R., Zambrano-Bigiarini, M., Alvarez-Garreton, C., Baez-Villanueva, O.M., Sheffield, J. and Karger, D.N. (2020) Bias correction of global high-resolution precipitation climatologies using streamflow observations from 9372 catchments. *Journal of Climate*, 33(4), 1299–1315. <http://doi.org/10.1175/jcli-d-19-0332.1>
- Bobrowski, M., Weidinger, J. and Schickhoff, U. (2021) Is new always better? Frontiers in global climate datasets for modeling treeline species in the Himalayas. *Atmosphere*, 12, 543. <https://doi.org/10.3390/atmos12050543>.
- Bonan, G.B. (2008) Forests and climate change: forcings, feedbacks, and the climate benefits of forests. *Science*, 320, 1444–1449. <https://doi.org/10.1126/science.1155121>.
- Bookhagen, B. and Strecker, M.R. (2008) Orographic barriers, high-resolution TRMM rainfall, and relief variations along the eastern Andes. *Geophysical Research Letters*, 35(6), <http://doi.org/10.1029/2007gl032011>
- Breheeny, P. and Burchett, W. (2017) Visualization of regression models using visreg. *R Journal*, 9, 56–71. <https://doi.org/10.32614/RJ-2017-046>.
- Bruijnzeel, L.A., Mulligan, M. and Scatena, F.N. (2011) Hydrometeorology of tropical montane cloud forests: emerging patterns. *Hydrological Processes*, 25, 465–498. <https://doi.org/10.1002/hyp.7974>.
- Butt, N., de Oliveira, P.A. and Costa, M.H. (2011) Evidence that deforestation affects the onset of the rainy season in Rondonia, Brazil. *Journal of Geophysical Research*, 116, D11120. <https://doi.org/10.1029/2010JD015174>.
- Chapman, S., Syktus, J., Trancoso, R., Salazar, A., Thatcher, M., Watson, J.E.M., Meijaard, E., Sheil, D., Dargusch, P. and McAlpine, C.A. (2020) Compounding impact of deforestation on Borneo's climate during El Niño events. *Environmental Research Letters*, 15, 084006. <https://doi.org/10.1088/1748-9326/ab86f5>.
- Chavez, S.P. and Takahashi, K. (2017) Orographic rainfall hot spots in the Andes-Amazon transition according to the TRMM precipitation radar and in situ data. *Journal of Geophysical Research: Atmospheres*, 122, 5870–5882. <https://doi.org/10.1002/2016JD026282>
- Colwell, R.K., Brehm, G., Cardelus, C.L., Gilman, A.C. and Longino, J.T. (2008) Global warming, elevational range shifts, and lowland biotic attrition in the wet tropics. *Science*, 322, 258–261. <https://doi.org/10.1126/science.1162547>.
- Cook, B.I., Smerdon, J.E., Seager, R. and Coats, S. (2014) Global warming and 21st century drying. *Climate Dynamics*, 43, 2607–2627. <https://doi.org/10.1007/s00382-014-2075-y>.
- Cox, D.T., Maclean, I.M., Gardner, A.S. and Gaston, K.J. (2020) Global variation in diurnal asymmetry in temperature, cloud cover, specific humidity and precipitation and its association with leaf area index. *Global Change Biology*, 26, 7099–7111. <https://doi.org/10.1111/gcb.15336>
- Crausbay, S.D., Frazier, A.G., Giambelluca, T.W., Longman, R.J. and Hotchkiss, S.C. (2014) Moisture status during a strong El

- Niño explains a tropical montane cloud forest's upper limit. *Oecologia*, 175, 273–284. <https://doi.org/10.1007/s00442-014-2888-8>.
- Davis, K.T., Dobrowski, S.Z., Holden, Z.A., Higuera, P.E. and Abatzoglou, J.T. (2019) Microclimatic buffering in forests of the future: the role of local water balance. *Ecography*, 42, 1–11. <https://doi.org/10.1111/ecog.03836>
- Davy, R., Esau, I., Chernokulsky, A., Outten, S. and Zilitinkevich, S. (2017) Diurnal asymmetry to the observed global warming. *International Journal of Climatology*, 37, 79–93. <https://doi.org/10.1002/joc.4688>
- De Frenne, P., Lenoir, J., Luoto, M., Scheffers, B.R., Zellweger, F., Aalto, J., Ashcroft, M.B., Christiansen, D.M., Decocq, G., De Pauw, K., Govaert, S., Greiser, C., Gril, E., Hampe, A., Jucker, T., Klings, D.H., Koelemeijer, I.A., Lembrechts, J.J., Marrec, R., Meeussen, C., Ogée, J., Tyystjärvi, V., Vangansbeke, P. and Hylander, K. (2021) Forest microclimates and climate change: importance, drivers and future research agenda. *Global Change Biology*, 27, 2279–2297. <https://doi.org/10.1111/gcb.15569>.
- De Frenne, P., Zellweger, F., Rodriguez-Sanchez, F., Scheffers, B.R., Hylander, K., Luoto, M., Vellend, M., Verheyen, K. and Lenoir, J. (2019) Global buffering of temperatures under forest canopies. *Nature Ecology & Evolution*, 3, 744–749. <https://doi.org/10.1038/s41559-019-0842-1>.
- de Oliveira-Júnior, J.F., Correia Filho, W.L.F., de Barros Santiago, D., de Gois, G., da Silva Costa, M., da Silva Junior, C. A., Teodoro, P.E. and Freire, F.M. (2021) Rainfall in Brazilian northeast via in situ data and CHELSA product: mapping, trends, and socio-environmental implications. *Environmental Monitoring and Assessment*, 193, 263. <https://doi.org/10.1007/s10661-021-09043-9>.
- de Sousa, K., Sparks, A.H., Ashmall, W., van Etten, J. and Solberg, S. (2020) chirps: API client for the CHIRPS precipitation data in R. *Journal of Open Source Software*, 5, 2419. <https://doi.org/10.21105/joss.02419>.
- Domínguez-Castro, F., Vicente-Serrano, S.M., López-Moreno, J.I., Correa, K., Ávalos, G., Azorin-Molina, C., El Kenawy, A., Tomas-Burguera, M., Navarro-Serrano, F., Peña-Gallardo, M., Gimeno, L. and Nieto, R. (2018) Mapping seasonal and annual extreme precipitation over the Peruvian Andes. *International Journal of Climatology*, 38, 5459–5475. <https://doi.org/10.1002/joc.5739>.
- Dowle, M. and Srinivasan, A. (2020) Data.table: extension of “data.frame.” R package version 1.13.0. <https://CRAN.R-project.org/package=data.table>
- Duane, W.J., Pepin, N.C., Losleben, M.L. and Hardy, D.R. (2008) General characteristics of temperature and humidity variability on Kilimanjaro, Tanzania. *Arctic, Antarctic, and Alpine Research*, 40, 323–334. [https://doi.org/10.1657/1523-0430\(06-127\)\[DUANE\]2.0.CO;2](https://doi.org/10.1657/1523-0430(06-127)[DUANE]2.0.CO;2).
- Ellison, D., Morris, C.E., Locatelli, B., Sheil, D., Cohen, J., Murdiyarso, D., Gutierrez, V., van Noordwijk, M., Creed, I.F., Pokorny, J., Gaveau, D., Spracklen, D.V., Tobella, A.B., Ilstedt, U., Teuling, A.J., Gebrehiwot, S.G., Sands, D.C., Muys, B., Verbist, B., Springgay, E., Sugandi, Y. and Sullivan, C.A. (2017) Trees, forests and water: Cool insights for a hot world. *Global Environmental Change*, 43, 51–61. <https://doi.org/10.1016/j.gloenvcha.2017.01.002>.
- Espinoza Villar, J.C., Ronchail, J., Guyot, J.L., Cochonneau, G., Naziano, F., Lavado, W., De Oliveira, E., Pombosa, R. and Vauchel, P. (2009) Spatio-temporal rainfall variability in the Amazon basin countries (Brazil, Peru, Bolivia, Colombia, and Ecuador). *International Journal of Climatology*, 29, 1574–1594. <https://doi.org/10.1002/joc.1791>
- Fadrique, B., Báez, S., Duque, Á., Malizia, A., Blundo, C., Carilla, J., Osinaga-Acosta, O., Malizia, L., Silman, M., Farfán-Ríos, W., Malhi, Y., Young, K.R., Cuesta, C.F., Homeier, J., Peralvo, M., Pinto, E., Jadan, O., Aguirre, N., Aguirre, Z. and Feeley, K.J. (2018) Widespread but heterogeneous responses of Andean forests to climate change. *Nature*, 564, 207–212. <https://doi.org/10.1038/s41586-018-0715-9>.
- Faye, E., Herrera, M., Bellomo, L., Silvain, J.-F. and Dangles, O. (2014) Strong discrepancies between local temperature mapping and interpolated climatic grids in tropical mountainous agricultural landscapes. *PLoS One*, 9, e105541. <https://doi.org/10.1371/journal.pone.0105541>.
- Feeley, K.J., Bravo-Avila, C., Fadrique, B., Perez, T.M. and Zuleta, D. (2020) Climate-driven changes in the composition of New World plant communities. *Nature Climate Change*, 10, 965–970. <https://doi.org/10.1038/s41558-020-0873-2>.
- Feeley, K.J., Silman, M.R., Bush, M.B., Farfan, W., Cabrera, K.G., Malhi, Y., Meir, P., Revilla, N.S., Quisipyanqui, M.N.R. and Saatchi, S. (2011) Upslope migration of Andean trees. *Journal of Biogeography*, 38, 783–791. <https://doi.org/10.1111/j.1365-2699.2010.02444.x>.
- Fick, S.E. and Hijmans, R.J. (2017) WorldClim 2: new 1-km spatial resolution climate surfaces for global land areas. *International Journal of Climatology*, 37, 4302–4315. <https://doi.org/10.1002/joc.5086>.
- Forero-Medina, G., Terborgh, J., Socolar, S.J. and Pimm, S.L. (2011) Elevational ranges of birds on a tropical montane gradient lag behind warming temperatures. *PLoS One*, 6, e28535. <https://doi.org/10.1371/journal.pone.0028535>.
- Foster, P. (2001) The potential negative impacts of global climate change on tropical montane cloud forests. *Earth-Science Reviews*, 55, 73–106. [https://doi.org/10.1016/S0012-8252\(01\)00056-3](https://doi.org/10.1016/S0012-8252(01)00056-3).
- Freeman, B.G. and Class Freeman, A.M. (2014) Rapid upslope shifts in new Guinean birds illustrate strong distributional responses of tropical montane species to global warming. *Proceedings of the National Academy of Sciences of the United States of America*, 111, 4490–4494. <https://doi.org/10.1073/pnas.1318190111>.
- Freeman, B.G., Lee-Yaw, J.A., Sunday, J.M. and Hargreaves, A.L. (2018) Expanding, shifting and shrinking: The impact of global warming on species' elevational distributions. *Global Ecology and Biogeography*, 27, 1268–1276. <https://doi.org/10.1111/geb.12774>.
- Freeman, B.G., Song, Y., Feeley, K.J. and Zhu, K. (2021) Montane species track rising temperatures better in the tropics than in the temperate zone. *Ecology Letters*, 24, 1697–1708. <https://doi.org/10.1111/ele.13762>.
- Fries, A., Rollenbeck, R., Göttlicher, D., Nauß, T., Homeier, J., Peters, T. and Bendix, J. (2009) Thermal structure of a megadiverse Andean mountain ecosystem in southern Ecuador and its regionalization. *Erdkunde*, 63, 321–335. <https://doi.org/10.3112/erdkunde.2009.04.03>.

- Fu, R., Yin, L., Li, W., Arias, P.A., Dickinson, R.E., Huang, L., Chakraborty, S., Fernandes, K., Liebmann, B., Fisher, R. and Myneni, R.B. (2013) Increased dry-season length over southern Amazonia in recent decades and its implication for future climate projection. *Proceedings of the National Academy of Sciences of the United States of America*, 110, 18110–18115. <https://doi.org/10.1073/pnas.1302584110>.
- Funk, C., Peterson, P., Landsfeld, M., Pedreros, D., Verdin, J., Shukla, S., Husak, G., Rowland, J., Harrison, L., Hoell, A. and Michaelsen, J. (2015) The climate hazards infrared precipitation with stations—a new environmental record for monitoring extremes. *Scientific Data*, 2, 150066. <https://doi.org/10.1038/sdata.2015.66>.
- Giambelluca, T.W. and Gerold, G. (2011) Hydrology and biogeochemistry of tropical montane cloud forests. In: Levia, D., Carlyle-Moses, D. and Tanaka, T. (eds), *Forest Hydrology and Biogeochemistry. Ecological Studies (Analysis and Synthesis)*, vol. 216. Springer, Dordrecht. https://doi.org/10.1007/978-94-007-1363-5_11
- Gimeno, L., Vázquez, M., Eiras-Barca, J., Sorí, R., Stojanovic, M., Algarra, I., Nieto, R., Ramos, A.M., Durán-Quesada, A.M. and Dominguez, F. (2020) Recent progress on the sources of continental precipitation as revealed by moisture transport analysis. *Earth-Science Reviews*, 201, 103070. <https://doi.org/10.1016/j.earscirev.2019.103070>.
- Gotsch, S.G., Davidson, K., Murray, J.G., Duarte, V.J. and Draguljić, D. (2017) Vapor pressure deficit predicts epiphyte abundance across an elevational gradient in a tropical montane region. *American Journal of Botany*, 104, 1790–1801. <https://doi.org/10.3732/ajb.1700247>.
- Grossiord, C., Buckley, T.N., Cernusak, L.A., Novick, K.A., Poulter, B., Siegwolf, R.T.W., Sperry, J.S. and McDowell, N.G. (2020) Plant responses to rising vapor pressure deficit. *New Phytologist*, 226, 1550–1566. <https://doi.org/10.1111/nph.16485>.
- Hamner, B., Frasco, M. and LeDell, E. (2018) Metrics: Evaluation metrics for machine learning. R package version 0.1.4. <https://CRAN.R-project.org/package=Metrics>
- Hardwick, S.R., Toumi, R., Pfeifer, M., Turner, E.C., Nilus, R. and Ewers, R.M. (2015) The relationship between leaf area index and microclimate in tropical forest and oil palm plantation: forest disturbance drives changes in microclimate. *Agricultural and Forest Meteorology*, 201, 187–195. <https://doi.org/10.1016/j.agrformet.2014.11.010>.
- Hazzi, N.A., Moreno, J.S., Ortiz-Movliav, C. and Palacio, R.D. (2018) Biogeographic regions and events of isolation and diversification of the endemic biota of the tropical Andes. *Proceedings of the National Academy of Sciences of the United States of America*, 115, 7985–7990. <https://doi.org/10.1073/pnas.1803908115>.
- Held, I.M., Soden, B.J. (2006) Robust responses of the hydrological cycle to global warming. *Journal of Climate*, 19(21), 5686–5699. <http://doi.org/10.1175/jcli3990.1>
- Helmer, E.H., Gerson, E.A., Baggett, L.S., Bird, B.J., Ruzycski, T.S. and Voggesser, S.M. (2019) Neotropical cloud forests and páramo to contract and dry from declines in cloud immersion and frost. *PLoS One*, 14, e0213155. <https://doi.org/10.1371/journal.pone.0213155>.
- Hijmans, R.J. (2021) raster: Geographic data analysis and modeling. R package version 3.4-10. <https://CRAN.R-project.org/package=raster>
- Hijmans, R.J., Cameron, S.E., Parra, J.L., Jones, P.G. and Jarvis, A. (2005) Very high resolution interpolated climate surfaces for global land areas. *International Journal of Climatology*, 25, 1965–1978. <https://doi.org/10.1002/joc.1276>.
- Huffman, G.J., Bolvin, D.T., Braithwaite, D., Hsu, K., Joyce, R., Kidd, C., Nelkin, E.J., Sorooshian, S., Tan, J. and Xie, P. (2020) NASA global precipitation measurement (GPM) integrated multi-satellite retrievals for GPM (IMERG), algorithm theoretical basis document (ATBD). <https://gpm.nasa.gov/resources/documents/algorithm-information/IMERG-V06-ATBD>
- Husak, G.J., Michaelsen, J. and Funk, C. (2007) Use of the gamma distribution to represent monthly rainfall in Africa for drought monitoring applications. *International Journal of Climatology*, 27, 935–944. <https://doi.org/10.1002/joc.1441>
- Ives, A.R. and Li, D. (2018) rr2: An R package to calculate R²s for regression models. *Journal of Open Source Software*, 3, 1028. <https://doi.org/10.21105/joss.01028>
- Jasechko, S., Sharp, Z.D., Gibson, J.J., Birks, S.J., Yi, Y. and Fawcett, P.J. (2013) Terrestrial water fluxes dominated by transpiration. *Nature*, 496, 347–350. <https://doi.org/10.1038/nature11983>.
- Jucker, T., Hardwick, S.R., Both, S., Elias, D.M.O., Ewers, R.M., Milodowski, D.T., Swinfield, T. and Coomes, D.A. (2018) Canopy structure and topography jointly constrain the microclimate of human-modified tropical landscapes. *Global Change Biology*, 24, 5243–5258. <https://doi.org/10.1111/gcb.14415>.
- Junquas, C., Takahashi, K., Condom, T., Espinoza, J.-C., Chavez, S., Sicart, J.-E. and Lebel, T. (2018) Understanding the influence of orography on the precipitation diurnal cycle and the associated atmospheric processes in the Central Andes. *Climate Dynamics*, 50, 3995–4017. <https://doi.org/10.1007/s00382-017-3858-8>.
- Karger, D.N., Conrad, O., Böhner, J., Kawohl, T., Kreft, H., Soria-Auza, R.W., Zimmermann, N.E., Linder, H.P. and Kessler, M. (2017) Climatologies at high resolution for the earth's land surface areas. *Scientific Data*, 4, 170122. <https://doi.org/10.1038/sdata.2017.122>.
- Karger, D.N., Conrad, O., Böhner, J., Kawohl, T., Kreft, H., Soria-Auza, R.W., Zimmermann, N.E., Linder, H.P. and Kessler, M. (2021) Data from: Climatologies at high resolution for the earth's land surface areas. EnviDat Digital Repository. <https://doi.org/10.16904/envi.dat.228.v2.1>
- Karmalkar, A.V., Bradley, R.S. and Diaz, H.F. (2008) Climate change scenario for Costa Rican montane forests. *Geophysical Research Letters*, 35, L11702. <https://doi.org/10.1029/2008GL033940>.
- Killeen, T.J., Douglas, M., Consiglio, T., Jørgensen, P.M. and Mejia, J. (2007) Dry spots and wet spots in the Andean hotspot. *Journal of Biogeography*, 34(8), 1357–1373. <http://doi.org/10.1111/j.1365-2699.2006.01682.x>
- Knoben, W.J., Woods, R.A. and Freer, J.E. (2019) Global bimodal precipitation seasonality: A systematic overview. *International Journal of Climatology*, 39, 558–567. <https://doi.org/10.1002/joc.5786>
- Körner, C. (2007) The use of “altitude” in ecological research. *Trends in Ecology & Evolution*, 22, 569–574. <https://doi.org/10.1016/j.tree.2007.09.006>.

- Laraque, A., Ronchail, J., Cochonneau, G., Pombosa, R. and Guyot, J.L. (2007) Heterogeneous distribution of rainfall and discharge regimes in the Ecuadorian Amazon Basin. *Journal of Hydrometeorology*, 8, 1364–1381. <https://doi.org/10.1175/2007JHM784.1>.
- Leite-Filho, A.T., Sousa Pontes, V.Y. and Costa, M.H. (2019) Effects of deforestation on the onset of the rainy season and the duration of dry spells in southern Amazonia. *Journal of Geophysical Research: Atmospheres*, 124, 5268–5281. <https://doi.org/10.1029/2018JD029537>.
- Lembrechts, J.J., Lenoir, J., Roth, N., Hattab, T., Milbau, A., Haider, S., Pellissier, L., Pauchard, A., Ratier Backes, A., Dimarco, R.D., Nuñez, M.A., Aalto, J. and Nijs, I. (2019) Comparing temperature data sources for use in species distribution models: From in-situ logging to remote sensing. *Global Ecology and Biogeography*, 28, 1578–1596. <https://doi.org/10.1111/geb.12974>.
- Lenoir, J. and Svenning, J.C. (2015) Climate-related range shifts—a global multidimensional synthesis and new research directions. *Ecography*, 38, 15–28. <https://doi.org/10.1111/ecog.00967>.
- Lenth, R.V. (2021) emmeans: Estimated Marginal Means, aka Least-Squares Means. R package version 1.6.0. <https://CRAN.R-project.org/package=emmeans>
- Li, Y., Zhao, M., Motesharrei, S., Mu, Q., Kalnay, E. and Li, S. (2015) Local cooling and warming effects of forests based on satellite observations. *Nature Communications*, 6, 6603. <https://doi.org/10.1038/ncomms7603>.
- Lute, A.C. and Abatzoglou, J.T. (2021) Best practices for estimating near-surface air temperature lapse rates. *International Journal of Climatology*, 41, E110–E125. <https://doi.org/10.1002/joc.6668>.
- Mair, A. and Fares, A. (2010) Assessing rainfall data homogeneity and estimating missing records in Mākaha Valley, O'ahu, Hawai'i. *Journal of Hydrologic Engineering*, 15, 61–66. [https://doi.org/10.1061/\(ASCE\)HE.1943-5584.0000145](https://doi.org/10.1061/(ASCE)HE.1943-5584.0000145).
- Makarieva, A.M. and Gorshkov, V.G. (2007) Biotic pump of atmospheric moisture as driver of the hydrological cycle on land. *Hydrology and Earth System Sciences*, 11(2), 1013–1033. <http://doi.org/10.5194/hess-11-1013-2007>
- McCain, C.M. and Colwell, R.K. (2011) Assessing the threat to montane biodiversity from discordant shifts in temperature and precipitation in a changing climate: climate change risk for montane vertebrates. *Ecology Letters*, 14, 1236–1245. <https://doi.org/10.1111/j.1461-0248.2011.01695.x>.
- Meyer, D. and Thevenard, D. (2019) PsychroLib: a library of psychrometric functions to calculate thermodynamic properties of air. *Journal of Open Source Software*, 4, 1137. <https://doi.org/10.21105/joss.01137>.
- Mohammadi, B., Vaheddoost, B. and Danandeh Mehr, A. (2020) A spatiotemporal teleconnection study between Peruvian precipitation and oceanic oscillations. *Quaternary International*, 565, 1–11. <https://doi.org/10.1016/j.quaint.2020.09.042>.
- Monteith, J.L. (1965) Evaporation and environment. In: *Symposia of the Society for Experimental Biology*. Cambridge: Cambridge University Press, pp. 205–234.
- Montejo-Kovacevich, G., Martin, S.H., Meier, J.I., Bacquet, C.N., Monllor, M., Jiggins, C.D. and Nadeau, N.J. (2020) Microclimate buffering and thermal tolerance across elevations in a tropical butterfly. *Journal of Experimental Biology*, 223, jeb220426. <https://doi.org/10.1242/jeb.220426>.
- Mutke, J., Böhnert, T. and Weigend, M. (2017) Save last cloud forests in western Andes. *Nature*, 541, 157–157. <https://doi.org/10.1038/541157e>.
- Myers, N., Mittermeier, R.A., Mittermeier, C.G., da Fonseca, G.A.B. and Kent, J. (2000) Biodiversity hotspots for conservation priorities. *Nature*, 403(6772), 853–858. <http://doi.org/10.1038/35002501>
- Nadkarni, N.M. and Solano, R. (2002) Potential effects of climate change on canopy communities in a tropical cloud forest: An experimental approach. *Oecologia*, 131, 580–586. <https://doi.org/10.1007/s00442-002-0899-3>
- Nakamura, A., Kitching, R.L., Cao, M., Creedy, T.J., Fayle, T.M., Freiberg, M., Hewitt, C.N., Itioka, T., Koh, L.P., Ma, K., Malhi, Y., Mitchell, A., Novotny, V., Ozanne, C.M.P., Song, L., Wang, H. and Ashton, L.A. (2017) Forests and their canopies: Achievements and horizons in canopy science. *Trends in Ecology & Evolution*, 32, 438–451. <https://doi.org/10.1016/j.tree.2017.02.020>.
- Navarro-Serrano, F., López-Moreno, J.I., Domínguez-Castro, F., Alonso-González, E., Azorin-Molina, C., El-Kenawy, A. and Vicente-Serrano, S.M. (2020) Maximum and minimum air temperature lapse rates in the Andean region of Ecuador and Peru. *International Journal of Climatology*, 40, 6150–6168. <https://doi.org/10.1002/joc.6574>.
- Newell, F.L. (2021) *Birds, arthropods, and plants: how rainfall seasonality regulates reproduction across food webs in the Peruvian Andes*. PhD Thesis. University of Florida.
- Newell, F.L., Ausprey, I.J. and Robinson, S.K. Data from: Spatiotemporal climate variability in the Andes of northern Peru: Evaluation of gridded datasets to describe cloud forest microclimate and local rainfall. Figshare Digital Repository. <https://doi.org/10.6084/m9.figshare.18543167>
- O'Connor, J.C., Dekker, S.C., Staal, A., Tuinenburg, O.A., Rebel, K. T. and Santos, M.J. (2021) Forests buffer against variations in precipitation. *Global Change Biology*, 27, 4686–4696. <https://doi.org/10.1111/gcb.15763>.
- Padrón, R.S., Gudmundsson, L., Decharme, B., Ducharme, A., Lawrence, D.M., Mao, J., Peano, D., Krinner, G., Kim, H. and Seneviratne, S.I. (2020) Observed changes in dry-season water availability attributed to human-induced climate change. *Nature Geoscience*, 13, 477–481. <https://doi.org/10.1038/s41561-020-0594-1>.
- Paulhus, J.L. and Kohler, M.A. (1952) Interpolation of missing precipitation records. *Monthly Weather Review*, 80, 129–133. [https://doi.org/10.1175/1520-0493\(1952\)080<0129:IOMPR>2.0.CO;2](https://doi.org/10.1175/1520-0493(1952)080<0129:IOMPR>2.0.CO;2).
- Peixoto, J.P. and Oort, A.H. (1996) The climatology of relative humidity in the atmosphere. *Journal of Climate*, 9, 3443–3463. [https://doi.org/10.1175/1520-0442\(1996\)009<3443:TCORHI>2.0.CO;2](https://doi.org/10.1175/1520-0442(1996)009<3443:TCORHI>2.0.CO;2)
- Penman, H.L. (1948) Natural evaporation from open water, bare soil and grass. *Proceedings of the Royal Society of London. Series A. Mathematical and Physical Sciences*, 193, 120–145. <https://doi.org/10.1098/rspa.1948.0037>.
- Pielke, R.A., Adegoke, J., Beltraán-Przekurat, A., Hiemstra, C.A., Lin, J., Nair, U.S., Niyogi, D., and Nobis, T.E. (2007) An overview of regional land-use and land-cover impacts on rainfall. *Tellus B: Chemical and Physical Meteorology*, 59(3), 587–601. <http://doi.org/10.1111/j.1600-0889.2007.00251.x>
- Pierce, D. (2019) ncd4: Interface to Unidata netCDF (Version 4 or Earlier) Format Data Files. R package version 1.17. <https://CRAN.R-project.org/package=ncdf4>

- Ponce-Reyes, R., Reynoso-Rosales, V.H., Watson, J.E.M., VanDerWal, J., Fuller, R.A., Pressey, R.L., Possingham, H.P. (2012) Vulnerability of cloud forest reserves in Mexico to climate change. *Nature Climate Change*, 2(6), 448–452. <http://doi.org/10.1038/nclimate1453>
- Pounds, J.A., Fogden, M.P. L., Campbell, J.H. (1999) Biological response to climate change on a tropical mountain. *Nature*, 398 (6728), 611–615. <https://doi.org/10.1038/19297>
- Poveda, G., Espinoza, J.C., Zuluaga, M.D., Solman, S.A., Garreaud Salazar, R. and van Oevelen, P.J. (2020) High impact weather events in the Andes. *Frontiers in Earth Science*, 8, 1–32. <https://doi.org/10.3389/feart.2020.00162>
- Rahbek, C., Borregaard, M.K., Colwell, R.K., Dalsgaard, B., Holt, B.G., Morueta-Holme, N., Nogues-Bravo, D., Whittaker, R.J. and Fjeldsø, J. (2019) Humboldt's enigma: What causes global patterns of mountain biodiversity? *Science*, 365(6458), 1108–1113. <http://doi.org/10.1126/science.aax0149>
- Ramírez, B.H., Teuling, A.J., Ganzeveld, L., Hegger, Z. and Leemans, R. (2017) Tropical montane cloud forests: hydrometeorological variability in three neighbouring catchments with different forest cover. *Journal of Hydrology*, 552, 151–167. <https://doi.org/10.1016/j.jhydrol.2017.06.023>
- Rapp, J. and Silman, M. (2012) Diurnal, seasonal, and altitudinal trends in microclimate across a tropical montane cloud forest. *Climate Research*, 55, 17–32. <https://doi.org/10.3354/cr01127>
- Rascón, J., Gosgot Angeles, W., Quiñones Huatangari, L., Oliva, M. and Barrena Gurbillón, M.Á. (2021) Dry and wet events in Andean populations of northern Peru: a case study of Chachapoyas, Peru. *Frontiers in Environmental Science*, 9, 614438. <https://doi.org/10.3389/fenvs.2021.614438>
- Rifai, S.W., Li, S. and Malhi, Y. (2019) Coupling of El Niño events and long-term warming leads to pervasive climate extremes in the terrestrial tropics. *Environmental Research Letters*, 14(10), 105002. <http://doi.org/10.1088/1748-9326/ab402f>
- Rodríguez-Morata, C., Ballesteros-Canovas, J.A., Rohrer, M., Espinoza, J.C., Beniston, M. and Stoffel, M. (2018) Linking atmospheric circulation patterns with hydro-geomorphic disasters in Peru. *International Journal of Climatology*, 38, 3388–3404. <https://doi.org/10.1002/joc.5507>
- Rojas Briceño, N.B., Salas López, R., Silva López, J.O., Oliva-Cruz, M., Gómez Fernández, D., Terrones Murga, R.E., Iliquin Trigoso, D., Barrena Gurbillón, M. and Barboza, E. (2021) Site selection for a network of weather stations using AHP and near analysis in a GIS environment in Amazonas, NW Peru. *Climate*, 9, 169. <https://doi.org/10.3390/cli9120169>
- Rollenbeck, R. and Bendix, J. (2011) Rainfall distribution in the Andes of southern Ecuador derived from blending weather radar data and meteorological field observations. *Atmospheric Research*, 99, 277–289. <https://doi.org/10.1016/j.atmosres.2010.10.018>
- Schwärzel, K., Zhang, L., Montanarella, L., Wang, Y. and Sun, G. (2020) How afforestation affects the water cycle in drylands: a process-based comparative analysis. *Global Change Biology*, 26, 944–959. <https://doi.org/10.1111/gcb.14875>
- Segura, H., Junquas, C., Espinoza, J.C., Vuille, M., Jauregui, Y.R., Rabatel, A., Condom, T. and Lebel, T. (2019) New insights into the rainfall variability in the tropical Andes on seasonal and interannual time scales. *Climate Dynamics*, 53, 405–426. <https://doi.org/10.1007/s00382-018-4590-8>
- Sheil, D. (2018) Forests, atmospheric water and an uncertain future: the new biology of the global water cycle. *Forest Ecosystems*, 5, 19. <https://doi.org/10.1186/s40663-018-0138-y>
- Sherwood, S. and Fu, Q. (2014) A drier future? *Science*, 343, 737–739. <https://doi.org/10.1126/science.1247620>
- Spracklen, D.V., Arnold, S.R. and Taylor, C.M. (2012) Observations of increased tropical rainfall preceded by air passage over forests. *Nature*, 489, 282–285. <https://doi.org/10.1038/nature11390>
- Spracklen, D.V., Baker, J.C.A., Garcia-Carreras, L. and Marsham, J. H. (2018) The effects of tropical vegetation on rainfall. *Annual Review of Environment and Resources*, 43, 193–218. <https://doi.org/10.1146/annurev-environ-102017-030136>
- Staal, A., Tuinenburg, O.A., Bosmans, J.H.C., Holmgren, M., van Nes, E.H., Scheffer, M., Zemp, D.C., Dekker, S.C. (2018) Forest-rainfall cascades buffer against drought across the Amazon. *Nature Climate Change*, 8(6), 539–543. <http://doi.org/10.1038/s41558-018-0177-y>
- Still, C.J., Foster, P.N., Schneider, S.H. (1999) Simulating the effects of climate change on tropical montane cloud forests. *Nature*, 398(6728), 608–610. <http://doi.org/10.1038/19293>
- Thorntwaite, C.W. (1948) An approach toward a rational classification of climate. *Geographical Review*, 38(1), 55. <http://doi.org/10.2307/210739>
- Thorsten, P. trend: Non-parametric trend tests and change-point detection. R package version 1.1.4. <https://CRAN.R-project.org/package=trend>
- Urrutia, R. and Vuille, M. (2009) Climate change projections for the tropical Andes using a regional climate model: Temperature and precipitation simulations for the end of the 21st century. *Journal of Geophysical Research*, 114, D02108. <https://doi.org/10.1029/2008JD011021>
- Vermote, E. and Wolfe, R. (2015) MOD09GQ MODIS/Terra Surface Reflectance Daily L2G Global 250m SIN Grid. NASA GSFC and MODAPS SIPS - NASA LP DAAC. <http://doi.org/10.5067/MODIS/MOD09GQ.006>
- Vicente-Serrano, S.M., Beguería, S. and López-Moreno, J.I. (2010) A multiscalar drought index sensitive to global warming: The standardized precipitation evapotranspiration index. *Journal of Climate*, 23, 1696–1718. <https://doi.org/10.1175/2009JCLI2909.1>
- Vicente-Serrano, S.M., Quiring, S.M., Peña-Gallardo, M., Yuan, S. and Domínguez-Castro, F. (2020) A review of environmental droughts: increased risk under global warming? *Earth-Science Reviews*, 201, 102953. <https://doi.org/10.1016/j.earscirev.2019.102953>
- Weigend, M. (2002) Observations on the biogeography of the Amotape-Huancabamba zone in northern Peru. *Botanical Review*, 68, 38–54. [https://doi.org/10.1663/0006-8101\(2002\)068\[0038:OOTBOT\]2.0.CO;2](https://doi.org/10.1663/0006-8101(2002)068[0038:OOTBOT]2.0.CO;2)
- Wood, S. and Scheipl, F. (2020) gamm4: generalized additive mixed models using “mgcv” and “lme4.” R package version 0.2-6. <https://CRAN.R-project.org/package=gamm4>
- Xu, X., Jia, G., Zhang, X., Riley, W.J. and Xue, Y. (2020) Climate regime shift and forest loss amplify fire in Amazonian forests. *Global Change Biology*, 26, 5874–5885. <https://doi.org/10.1111/gcb.15279>
- Yuan, W., Zheng, Y., Piao, S., Ciais, P., Lombardozzi, D., Wang, Y., Ryu, Y., Chen, G., Dong, W., Hu, Z., Jain, A.K., Jiang, C., Kato, E., Li, S., Lienert, S., Liu, S., Nabel, J.E.M.S., Qin, Z., Quine, T., Sitch, S., Smith, W.K., Wang, F., Wu, C., Xiao, Z.

- and Yang, S. (2019) Increased atmospheric vapor pressure deficit reduces global vegetation growth. *Science Advances*, 5, eaax1396. <https://doi.org/10.1126/sciadv.aax1396>.
- Zellweger, F., De Frenne, P., Lenoir, J., Vangansbeke, P., Verheyen, K., Bernhardt-Römermann, M., Baeten, L., Hédl, R., Berki, I., Brunet, J., Van Calster, H., Chudomelová, M., Decocq, G., Dirnböck, T., Durak, T., Heinken, T., Jaroszewicz, B., Kopecký, M., Máliš, F., Macek, M., Malicki, M., Naaf, T., Nagel, T.A., Ortmann-Ajkai, A., Petřík, P., Pielech, R., Reczyńska, K., Schmidt, W., Standovár, T., Świerkosz, K., Teleki, B., Vild, O., Wulf, M. and Coomes, D. (2020) Forest microclimate dynamics drive plant responses to warming. *Science*, 368, 772–775. <https://doi.org/10.1126/science.aba6880>.
- Zemp, D.C. and Rammig, A. (2014) On the importance of cascading moisture recycling in South America. *Atmospheric Chemistry and Physics*, 23, 13337–13359. <https://doi.org/10.5194/acp-14-13337-2014>
- Zemp, D.C., Schleussner, C.-F., Barbosa, H.M.J., Hirota, M., Montade, V., Sampaio, G., Staal, A., Wang-Erlandsson, L. and Rammig, A. (2017) Self-amplified Amazon forest loss due to vegetation-atmosphere feedbacks. *Nature Communications*, 8, 14681. <https://doi.org/10.1038/ncomms14681>.
- Zhang, W., Furtado, K., Wu, P., Zhou, T., Chadwick, R., Marzin, C., Rostron, J. and Sexton, D. (2021) Increasing precipitation variability on daily-to-multiyear time scales in a warmer world. *Science Advances*, 7, 31. <https://doi.org/10.1126/sciadv.abf8021>.

SUPPORTING INFORMATION

Additional supporting information may be found in the online version of the article at the publisher's website.

How to cite this article: Newell, F. L., Ausprey, I. J., & Robinson, S. K. (2022). Spatiotemporal climate variability in the Andes of northern Peru: Evaluation of gridded datasets to describe cloud forest microclimate and local rainfall. *International Journal of Climatology*, 42(11), 5892–5915. <https://doi.org/10.1002/joc.7567>